Available online at www.sciencedirect.com
ScienceDirect
Deep-Sea Research I 54 (2007) 951–974
DEEP-SEA RESEARCH PART I
www.elsevier.com/locate/dsri

New estimates of Southern Ocean biological production rates from O_2/Ar ratios and the triple isotope composition of O_2

Matthew K. Reuer[a,*], Bruce A. Barnett[a], Michael L. Bender[a], Paul G. Falkowski[b], Melissa B. Hendricks[a]

[a]*Department of Geosciences, Guyot Hall, Princeton University, Princeton, NJ 08544-1003, USA*
[b]*Institute of Marine and Coastal Sciences, Rutgers University, 71 Dudley Road, New Brunswick, NJ 08901-8521, USA*

Received 6 April 2005; received in revised form 20 February 2007; accepted 23 February 2007
Available online 12 March 2007

Abstract

We report O_2/Ar ratios (a constraint on net community production) and the triple isotopic composition of dissolved O_2 (a constraint on gross primary production) in samples collected from the surface mixed layer on 23 Southern Ocean transits. Samples were collected at 1–2° meridional resolution during the austral summer. Methodological limitations notwithstanding, the results constrain the net/gross production ratio, net O_2 production, and gross O_2 production at unprecedented resolution throughout the Southern Ocean mixed layer. Gross O_2 production rates inferred from the oxygen triple isotopes are greater than production rates calculated from a model based on remotely sensed chlorophyll. This result agrees with previous ^{18}O and ^{14}C incubations along 170°W. O_2/Ar ratios exceeding saturation are consistently observed within the Subantarctic and Polar Frontal Zones south of New Zealand and Australia, showing that a net autotrophic community predominates during austral summer. Lower O_2/Ar values are observed within the Drake Passage and Antarctic Zone, suggesting unresolved influences of low net community production, net heterotrophy, and upwelling of O_2-undersaturated waters. In autotrophic waters of the austral summer mixed layer, ratios of net community production/gross O_2 production scatter about 0.13, corresponding to f ratios of ~0.25. Net community/gross O_2 production ratios show no meridional gradient across the Antarctic Circumpolar Current, suggesting that an approximately constant fraction of gross primary productivity is regenerated or exported. Our calculated net O_2 production rates are in satisfactory agreement with comparable published estimates. Net and gross O_2 production rates are highest in the Subantarctic and decline to the south, paralleling the well-known trend of chlorophyll *a* concentrations. In an analysis of variance of net O_2 production and gross O_2 production with other environmental variables, the strongest correlations are between net O_2 production and sea surface temperature (SST) (direct correlation), climatological [NO_3^-] (inverse correlation), and estimates of primary productivity derived from a remote sensing (direct correlation). These trends are as expected if aerosol iron input is the most important influence on production. They are unexpected if upwelling-derived SiO_2 and iron are the leading influence or if lower SSTs promote greater export in this region.
© 2007 Elsevier Ltd. All rights reserved.

Keywords: Dissolved gases; Oxygen isotopes; Primary production; Southern Ocean

*Corresponding author. Fax: +1 719 227 8229.
E-mail address: mreuer@coloradocollege.edu (M.K. Reuer).

0967-0637/$ - see front matter © 2007 Elsevier Ltd. All rights reserved.
doi:10.1016/j.dsr.2007.02.007

1. Introduction

Ecosystems of the Southern Ocean upper water column impact regional and global biogeochemistry in several important ways. Export production in this region efficiently transfers nutrients to the deep ocean, thereby influencing the initial concentrations of nitrate and phosphate within the intermediate waters and subtropical mode waters of the global oceans (Sarmiento et al., 2004). The Southern Ocean, particularly the region south of the Polar Front, also has an influence disproportionate to its area on glacial–interglacial CO_2 variability (Martin, 1990; Sigman and Boyle, 2000) and on the magnitude of the anthropogenic CO_2 transient. The Southern Ocean is the world's most extensive high nutrient-low chlorophyll region. Ecosystems of the Southern Ocean are clearly iron-limited (e.g., Boyd et al., 2000; Coale et al., 2004; Gervais et al., 2002, Buesseler et al., 2005), but limitation by grazing, SiO_2, and light may also attenuate export production and maintain the high inventory of dissolved nutrients.

The relative and absolute rates of net community production and gross production provide important information about the Southern Ocean carbon cycle. However, the modern variability of net and gross production remains poorly understood due to the difficulty of their experimental determination. The poor characterization of metabolic rates and their variability limits our ability to characterize the associated biogeochemical controls. Some definitions are appropriate here. *Gross O_2 production* is the rate at which O_2 is produced by the splitting of water. *Gross C production* is the rate at which CO_2 is fixed into organic C by the dark reactions of photosynthesis. *Net community O_2 production* is the difference between the rate of gross O_2 production and the rate of O_2 consumption by all metabolic processes (dark respiration, Mehler reaction, photorespiration, chlororespiration, alternative pathway, and nitrification). *Primary production* is operationally defined as ^{14}C production. *Net community C production* is the difference between the rate of gross C production and metabolic CO_2 release; it describes the net rate at which CO_2 is transformed to particulate and dissolved organic carbon (POC and DOC). In this paper, ''net production'' always refers to net community production (NCP). *New production* is the rate of NO_3^- assimilation (and the rate of CO_2 uptake supported by this assimilation). *Export production* is the rate at which POC and DOC are transferred from the euphotic zone to the dark ocean by sinking and subduction. At steady state, net O_2 production, net C production, new production and export production are assumed to be stoichiometrically equivalent. The justification for assuming this condition is that the increase in POC and DOC during the growing season is generally much less than net production.

Productivity models based on ocean color provide an important solution to characterizing Southern Ocean primary production, which can be determined using quasi-empirical models based on surface chlorophyll *a* concentrations, irradiance, and temperature (see Behrenfeld et al., 2002). Export production or NCP might also be quantified from ocean color data using simple temperature-dependent models as proposed by Laws et al. (2000). In this paper, we present a large suite of net and gross productivity observations from the Southern Ocean mixed layer, utilizing the stable isotopic composition of dissolved O_2 and elemental O_2/Ar ratios. Gross oxygen production rates are compared to an established satellite productivity model previously calibrated against ^{14}C uptake measurements (Behrenfeld and Falkowski, 1997). Net oxygen production rates are evaluated from mixed layer observations and compared with sea surface temperature (SST), surface irradiance, and nutrient concentrations. Finally, the net/gross ratio is compared to *f* ratio estimates determined from ^{15}N bottle incubations (Elskens et al., 2002; Sambrotto and Mace, 2000; Savoye et al., 2004) and the temperature-dependent model of Laws et al. (2000).

The net and gross production estimates presented here rely on two mixed layer dissolved gas tracers: the O_2/Ar ratio and the triple isotope composition of O_2 ($^{17}O/^{16}O$ and $^{18}O/^{16}O$, expressed as $\delta^{17}O$ and $\delta^{18}O$).[1] Argon provides a useful abiotic analog for dissolved O_2 given their similar solubilities (Craig and Hayward, 1987; Emerson, 1987; Quay et al., 1993; Spitzer and Jenkins, 1989). Mixed layer Ar is only affected by physical saturation mechanisms (e.g., bubble injection, atmospheric pressure variations, mixed layer warming) whereas O_2 responds to

[1]Throughout this work the delta notation is used to describe the stable oxygen isotopes, in units of per mil. For example, the $^{18}O/^{16}O$ ratio is defined according to the normalized departure from a compressed air reference standard: $\delta^{18}O = [(^{18}O/^{16}O)_{sample}/(^{18}O/^{16}O)_{standard} - 1] * 1000$.

both biological and physical mechanisms. By comparing the measured O_2/Ar ratio with the saturation ratio, one can estimate the biological contribution to the O_2 saturation. Net oxygen production rates are calculated by estimating the gas transfer velocity from wind speed observations (e.g., the quadratic model of Wanninkhof, 1992), providing a "clock" for the rate estimates. Equating the air–sea O_2 flux with net production assumes that recent rates of net production have been constant.

The approach of constraining gross O_2 production from the triple isotope composition of O_2, pioneered by Luz and Barkan (2000), is based on two isotopically distinct pools of O_2 dissolved in seawater: one deriving from air, and the other from photosynthesis in situ. The property that distinguishes these pools is the mass-independent anomaly in the isotopic composition of atmospheric O_2. The most accessible definition of this anomaly is:

$$\Delta^{17}O = \delta^{17}O - 0.52\delta^{18}O. \quad (1)$$

The (nominal) coefficient of 0.52 reflects the relative fractionation of the oxygen isotopes: nearly all geochemical reactions fractionate ^{17}O about half as much as ^{18}O relative to ^{16}O. We note here that other definitions have been suggested in the literature for describing the triple isotope composition of O_2. We use one of these terms, $^{17}\Delta$, later in the paper. For our samples, numerical values of $\Delta^{17}O$ and $^{17}\Delta$ are very similar.

The $\Delta^{17}O$ of atmospheric O_2 is different from water (and hence photosynthetic O_2) because of a mass-peculiar isotope exchange reaction in the stratosphere between O_2 and CO_2 (Thiemens and Heidenreich, 1983; Thiemens et al., 1995; Gao and Marcus, 2001; Lämmerzahl et al., 2002, Yung et al., 1997). Importantly, $\Delta^{17}O$ is not changed by respiration, which nominally discriminates against ^{17}O by 0.52 times as much as it discriminates against ^{18}O. This exchange, mediated by O_3, transfers ^{16}O to O_2 and the heavier isotopes to CO_2. Because of quantum mechanical effects during these reactions (e.g., Gao and Marcus, 2001), the fractionations are such that $\delta^{17}O$ of O_2 decreases by a factor of 1.7 relative to $\delta^{18}O$, rather than by a factor of 0.52 (Lämmerzahl et al., 2002). As a result, the triple isotope composition of O_2 in the global atmosphere is anomalous in that its ^{17}O abundance is lower than expected given its ^{18}O abundance. The isotopic composition of photosynthetic O_2 is identical to that of the source water (surface seawater in our case). $\Delta^{17}O$ of dissolved O_2 in the mixed layer is determined by the relative rates of photosynthesis (which adds isotopically normal O_2 from seawater) and gas exchange (which removes photosynthetic O_2, and replaces it with isotopically anomalous O_2 in air). One can thus calculate the rate of gross O_2 production in the mixed layer from the measured $\Delta^{17}O$ of O_2, along with the gas exchange coefficient estimated from wind speed. However, one must also account for the O_2 concentration; at a given rate of gross production, its $\Delta^{17}O$ signal will be smaller when the O_2 concentration is higher.

One can obviously calculate the net/gross O_2 production ratio from the values of net and gross production. One can also make this calculation given the geochemical measures of net and gross production (biological O_2 saturation and $\Delta^{17}O$ of O_2) in place of the rates derived from these terms. The net/gross O_2 production ratio is independent of gas exchange coefficient, and is therefore more accurately determined than the absolute rates. The ratio is comparable to the ratio of nitrate assimilation to total N assimilation (the *f* ratio of Eppley and Peterson, 1979), provided that one makes an appropriate stoichiometric correction.

In this paper, we first describe the methods used to estimate net and gross production rates: the oxygen triple isotope technique, the O_2/Ar measurement, and the parameterization of gas transfer velocities. The Southern Ocean mixed layer results are then presented, including the absolute and relative rates of net and gross oxygen production along 23 Southern Ocean transects. The observed meridional gradients in net and gross production and their significance are discussed, and the rates are compared to previous estimates from bottle incubations (^{14}C, ^{15}N, and ^{18}O), biogeochemical models, and seasonal nutrient and pCO_2 drawdown. The gross production rates are compared to estimates of primary production based on contemporaneous satellite-derived chlorophyll distributions using the algorithm described by Behrenfeld and Falkowski (1997).

2. Background

2.1. Absolute estimates of gross production and net community production

The relative and absolute rates of net community (N) and gross (G) oxygen production in the mixed layer are determined from the triple isotope composition of dissolved O_2 and O_2/Ar ratios,

assuming steady-state conditions. The N/G ratio is calculated directly from the concentration and isotopic data. Absolute production rates require gas exchange coefficients parameterized from wind speed observations. In this section, we present the methods for calculating absolute rates of net and gross production at steady state. In the next section we describe the calculation of gas exchange rate, and in the following section we outline the approach for calculating N/G.

Following Craig and Hayward (1987), the biological oxygen saturation is defined as

$$\Delta(O_2/Ar) = \left[\frac{(O_2/Ar)_{sample}}{(O_2/Ar)_{sat}} - 1\right], \quad (2)$$

where $(O_2/Ar)_{sample}$ is the measured seawater concentration ratio, $(O_2/Ar)_{sat}$ is the saturation concentration ratio determined from the solubility equations of Weiss (1970), and $\Delta(O_2/Ar)$ is the percent deviation of the measured O_2/Ar ratio from equilibrium. The net community oxygen production rate (N, units of mmol m^{-2} d^{-1}) can be calculated by

$$\text{Net community } O_2 \text{ production rate} = N = \Delta(O_2/Ar)[O_2]_{sat} k \rho, \quad (3)$$

where $\Delta(O_2/Ar)$ is defined above, $[O_2]_{sat}$ denotes the dissolved O_2 saturation concentration in units of μmol kg^{-1} (Weiss, 1970), k is the gas exchange coefficient (m day^{-1}, see below), and ρ denotes seawater density in units of kg L^{-1} (Millero and Poisson, 1981). Eq. (3) gives the instantaneous biological O_2 flux between the ocean and atmosphere. It equals export production if one assumes no mixing across the base of the mixed layer and one invokes steady-state conditions, wherein the net biological O_2 production equals the gas exchange flux.

Because the atmospheric O_2/Ar ratio (22.43, COESA, 1976) is 9% greater than the equilibrium O_2/Ar in seawater (20.47 at 10 °C, salinity = 35.0, Weiss, 1970), the mode of bubble injection may introduce a secondary error into these net oxygen production rates. Injection and complete dissolution of small bubbles into the mixed layer causes $\Delta(O_2/Ar)$ to increase according to the atmospheric ratio (Emerson et al., 1991; Spitzer and Jenkins, 1989). We neglect the small errors associated with this process.

Gross oxygen production rates can be determined from the oxygen triple isotopic composition of dissolved O_2 (^{16}O, ^{17}O, and ^{18}O). As described in the introduction, this approach relies on the change in $\delta^{17}O$ and $\delta^{18}O$ of dissolved O_2 as photosynthesis adds O_2 to the mixed layer reservoir, diminishing the magnitude of the ^{17}O anomaly associated with dissolved O_2 molecules from air. Photosynthesis adds O_2 with an isotopic composition identical to that of water (Guy et al., 1993; Luz and Barkan, 2005). As shown by Miller (2002), a useful expression for this anomaly is

$$^{17}\Delta = \left[\ln\left(\frac{\delta^{17}O}{1000} + 1\right) - \lambda \ln\left(\frac{\delta^{18}O}{1000} + 1\right)\right] 10^6, \quad (4)$$

where $\lambda = 0.516$ is the exact value characterizing the isotopic fractionation associated with dark respiration in a steady-state system (Angert et al., 2003). $^{17}\Delta$ is in units of per meg, and 1000 per meg = 1 per mil. Here and elsewhere (e.g., Luz and Barkan, 2000), studies of the triple isotope composition of O_2 adopt air O_2 as a standard. When all dissolved O_2 is atmospheric, $^{17}\Delta$ of dissolved O_2 is (nearly) identical to that of air. As photosynthesis adds O_2, the anomaly shifts towards the seawater value. Respiration does not cause $^{17}\Delta$ to change (Fig. 1).

Expressed more quantitatively, gas exchange reduces $^{17}\Delta$ towards the equilibrium value for

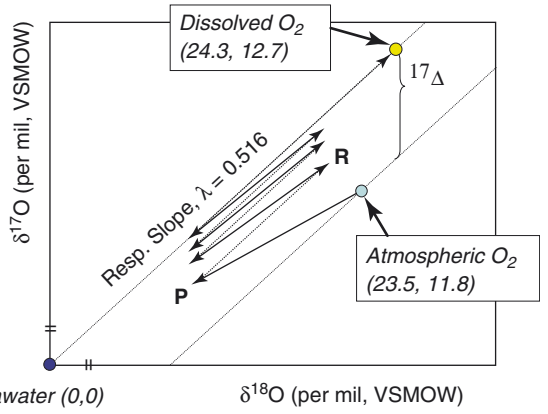

Fig. 1. Idealized schematic of O_2 triple isotope variations. The anomaly relative to air O_2 is generated by photosynthetic production of mass-dependent O_2 (passing through the seawater point) relative to mass-independent atmospheric O_2. This anomaly is equal to the vertical distance between the observed $\delta^{17}O$ and $\delta^{18}O$ values and a line with the slope shown, intersecting the atmospheric O_2 reference. Photosynthesis generates dissolved O_2 with $\delta^{18}O$ and $\delta^{17}O$ equal to zero due to water splitting by Photosystem II (solid vectors), increasing the anomaly with respect to air O_2. Respiration preferentially consumes ^{16}O, increasing both $\delta^{18}O$ and $\delta^{17}O$ with an assumed slope of $\lambda = 0.516$ (dashed vectors) and no change in the isotope anomaly. The scales here are vertically exaggerated and truncated.

dissolved O_2 (+8 per meg, see below). Photosynthesis increases $^{17}\Delta$ towards the hypothetical atmospheric value in the absence of the stratospheric influence. This value is the same as the $^{17}\Delta$ of seawater relative to modern air O_2: +249 per meg (Luz and Barkan, 2000). As shown by Luz and Barkan (2000), gross oxygen production rates can be directly determined by $^{17}\Delta$ observations, the assumed $^{17}\Delta$ of O_2 dissolved in seawater at equilibrium ($^{17}\Delta_{eq}$, +8 per meg), the assumed seawater $^{17}\Delta$ ($^{17}\Delta_{max}$, +249 per meg), the parameterized gas exchange coefficients, and dissolved [O_2] at saturation. For a steady-state mixed layer, gross production is most easily quantified with the ^{17}O and ^{18}O abundances expressed as $\Delta^{17}O$ (e.g. 1), with a coefficient of 0.516. Then to a good approximation (Hendricks et al., 2004):

$$P = k[O_2]_{sat}\left[\frac{\Delta^{17}O_{sat} - \Delta^{17}O_{dis}}{\Delta^{17}O_{dis} - \Delta^{17}O_{water}}\right] \quad (5)$$

This calculation is sensitive to errors in the measured $^{17}\Delta$ of dissolved O_2, the assumed $^{17}\Delta_{eq}$, and the gas exchange coefficient. The result is weakly sensitive to the saturation [O_2] and $^{17}\Delta_{water}$ (which $^{17}\Delta$ never approaches in the mixed layer). Our calculation assumes constant values of gross production and mixed layer thickness, but allows gas exchange to vary according to observed changes in windspeed (see below). The subscripts sat, dis, and w refer to dissolved O_2 at saturation, ambient dissolved O_2, and seawater.

The unapproximated version of Eq. (5) must be solved numerically (Hendricks et al., 2004). In the unapproximated version terms appear corresponding to the respiratory isotope fractionation factors (α's) for ^{17}O and ^{18}O and the $\delta^{17}O$ and $\delta^{18}O$ of atmospheric O_2. We adopted a value for the respiratory isotope fractionation of ^{18}O, α_{18}, of 0.980. This choice is a compromise between the bacterial isotope effect of ~0.982 (Kiddon et al., 1993) and the inferred isotope effect for ocean surface waters of 0.978 (Quay et al., 1993; Hendricks et al., 2004). α_{17} was calculated as $\alpha_{18}^{.516}$ (= 0.989630). The exponent agrees well (not perfectly) with the relationship between α_{17} and α_{18} determined recently by Luz and Barkan (2000). The $\delta^{18}O$ of atmospheric O_2 with respect to SMOW is +23.50‰ (Kroopnick and Craig, 1972). The corresponding atmospheric O_2 $\delta^{17}O$ value, calculated from Eq. (4), $\lambda = 0.516$, and $^{17}\Delta_{water} =$ 249 per meg, is 11.806‰. The resulting SMOW H_2O values with respect to atmospheric O_2 thus equal –22.960‰ (^{18}O) and −11.668‰ (^{17}O). These values all have geochemically significant uncertainties but these uncertainties introduce very little error into calculated values of gross production.

2.2. Calculation of gas exchange rates

Net community production and gross production estimates from $\Delta(O_2/Ar)$ and $^{17}\Delta$ observations rely on accurate gas transfer velocity estimates. To constrain this term, we require accurate Southern Ocean wind speed estimates and an associated gas exchange parameterization. We first examined the accuracy of the various wind speed products by comparison with relevant shipboard observations. Wind speeds from the NCEP/NCAR reanalysis model (Kalnay et al., 1996) and QuickScat scatterometer (e.g., Bourassa et al., 2003)[2] were compared to daily mean underway wind speeds for two Southern Ocean cruises (67°W and 169°E, $n = 29$ days). In each case, we evaluated three data products: (1) the daily mean NCEP/NCAR wind speed at the 0.995 sigma level (ca. 42 m), calculated as the mean of four instantaneous values every 6 h; (2) the daily mean NCEP/NCAR wind speed at 10 m, calculated as the mean of four 6-h forecasts; and (3) the daily mean 10 m QuickScat wind speed, calculated as the mean of 2 daily observations. The results of this comparison are shown in Table 1. QuickScat wind speeds showed best agreement with the underway observations, with a mean departure of −9% (17% maximum, −28% minimum). We therefore utilize the QuickScat results in this study.

Gas transfer velocities were then determined from daily 10 m wind speed observations (u_{10}) by the quadratic relationship of Wanninkhof (1992), calculating the Schmidt number (Sc) from SST observations ($k = 0.31 \cdot u_{10}^2 \cdot (Sc/660)^{-0.5}$). The biological O_2 concentration at the sample collection time depends on the prior net O_2 production (assumed to be constant) and prior wind speeds (known to be variable). We developed a simple weighting technique to account for the prior wind speed variability. First, the fraction of the mixed layer ventilated on the collection date (f_1) was determined from the climatological mixed layer

[2]The NCEP/NCAR reanalysis data were provided by the NOAA-CIRES Climate Diagnostics Center, Boulder, Colorado, USA, from their web site at http://www.cdc.noaa.gov. QuikScat data and images are produced by Remote Sensing Systems (http://www.ssmi.com) and sponsored by the NASA Ocean Vector Winds Science Team.

Table 1
Wind speed comparison for three data products, calculated as the percent departure from daily mean underway wind speed observations ($n = 29$ days)

Data Series	NCEP/NCAR reanalysis		QuickScat
Product	10 m, model-observed (%)	Sigma 0.995, model-observed (%)	10 m, model-observed (%)
Mean	−26	−22	−9
Maximum	24	81	17
Minimum	−70	−84	−28

Quickscat winds show better agreement. See text for data product definitions.

depths (Z_{mix}, Levitus and Boyer, 1994) and the gas transfer velocity on the collection day (k_1), and calculated as $f_1 = k_1 \cdot 1\,\text{day}/Z_{mix}$. The sample collection date was assigned a weight (ω_1) equal to 1. The fraction of the mixed layer ventilated on the day prior to sample collection (day 2) is similarly $f_2 = k_2 \cdot 1\,\text{day}/Z_{mix}$. The weight for this value is reduced according to the fraction of the mixed layer ventilated on day 1 ($\omega_2 = \omega_1(1-f_1)$). The general term for the weight on the tth day prior to sampling is $\omega_t = \omega_{t-1}(1-f_{t-1})$. By calculating a weighted gas transfer velocity for each day ($k_t\omega_t$), the weighted gas exchange rate for the mixed layer can be calculated as

$$k = \frac{\Sigma_{t=1}^{60} k_t \omega_t}{(1-\omega_{60})\Sigma_{t=1}^{60}\omega_t}, \quad (6)$$

where the $(1-\omega_{60})$ term accounts for the residual unventilated portion of the mixed layer and 60 days are utilized for each mixed layer station.

To test this technique, a simple box model calculation was performed for a hypothetical mixed layer depth (40 m), net O_2 production rate ($60\,\text{mmol}\,\text{m}^{-2}\,\text{d}^{-1}$), and initial dissolved [O_2] ($249.5\,\mu\text{mol}\,\text{kg}^{-1}$). Wind speeds were randomly varied between 1 and $20\,\text{m}\,\text{s}^{-1}$ and held constant for three-day periods. The weighting scheme was also compared to 7, 14, and 21 day averages. In each case, we compared the calculated net O_2 production rate (Eq. (2)) against the assigned value of $60\,\text{mmol}\,\text{m}^{-2}\,\text{d}^{-1}$. Net community production estimates agreed very well (−0.4% to +1.4%) when calculated as described above from the weighted k values. On the other hand, values of NCP calculated from mean wind speeds during the 7 days prior to collection were significantly offset from the assigned value (−89% to +71%). This simple calculation suggests the weighted gas transfer velocity provides a more robust estimate given the large variability in Southern Ocean wind speeds. However, there are other sources of error not addressed by this simple model. We do not account for time dependence in mixed layer thickness or net production. In any case, analytical errors and uncertainties in instantaneous gas transfer velocities remain the largest source of uncertainty.

2.3. Relative rates of net community production and gross photosynthesis

In Section 2.1, we show that the triple isotope composition of dissolved O_2, and the dissolved O_2/Ar ratio, constrain gross and NCP when evaluated using a windspeed parameterization. From this result, it is obvious that one can also calculate the ratio of net to gross production from the properties we measure. In this paper, we use two related approaches to evaluate this ratio. The first approach simply involves determining net and gross production as described above, and calculating the ratio. The second involves plotting $^{17}\Delta$ vs. O_2/Ar. The y-axis is then a measure of the fraction of dissolved O_2 derived from photosynthesis, while the x-axis is a measure of the fraction of excess O_2 derived from NCP. One can superimpose on this plot loci of $^{17}\Delta$–O_2/Ar points corresponding to different values of the gross production/gas exchange rate when values of net/gross production are held constant. These lines radiate from the equilibrium position. For ecosystems that are net autotrophic, they extend towards higher values of $^{17}\Delta$ and higher values of O_2/Ar. By comparing data points with net/gross production isolines, one can graphically constrain net/gross production in a sample. Uncertainties in the gas exchange parameterization introduce correlated errors in net and gross production. The calculated ratio of net/gross production is very nearly free of these errors.

2.4. Southern Ocean frontal boundaries

Across the Southern Ocean, there are several oceanographic fronts that separate distinct biogeographic provinces. From north to south, they include the Subtropical Front (STF), the Subantarctic Front (SAF), the Antarctic Polar Front (APF), the Southern Antarctic Circumpolar Current Front (SACCF), and the Southern Boundary of the ACC (SBACC). Ideally, the frontal positions are inferred from hydrographic sections across the ACC, best characterized by sharp gradients in potential density anomaly versus depth (see Fig. 9 of Orsi et al., 1995). However, this study necessarily relied on underway mixed layer observations. We adapted the criteria of Belkin and Gordon (1996, and references therein) to address this limitation, using the axial temperatures of 4 °C (APF) and 8 °C (SAF). Frontal positions were assigned according to their northern boundary rather than the absolute temperatures given seasonal SST variability. This approach yielded frontal boundaries consistent with Orsi et al. (1995), who calculated basin-scale frontal positions from a historical hydrographic compilation. For a December 2002 transit at 166°W, our SAF assignment (54.2°S) is within 2° of the Orsi et al. (1995) estimate (55.7°S), and the APF assignment (59.9°S) is within 1° of Orsi et al. (1995, 60.8°S). Exact agreement is not expected given interannual variability and offsets between mixed layer and hydrographic T, S gradients. Finally, the two southernmost fronts were ambiguous from mixed layer temperature and salinity observations alone. Thus, we refer to the entire region between the marginal ice zone (MIZ) and the Antarctic Polar Front (APF) as the Antarctic Zone (AZ). The MIZ is characterized by seasonally varying sea ice coverage, bounded to the north by the permanently open ocean zone (POOZ).

Along each of our sampling transits we report net and gross production rates for each station. We also tabulate average NCP rates, gross production rates, and N/G ratios for all samples of the transit lying within the Subantarctic Zone (SAF to STF), the Polar Frontal Zone (APF to SAF), and the Antarctic Zone (MIZ to APF) (Fig. 2).

3. Experimental methods

Mixed layer samples were collected from Niskin bottles and underway seawater pumping systems by collaborators aboard scientific ships of opportunity, crossing the Southern Ocean in austral summer. Sample collection dates are provided in Table 2, and the site locations are shown in Fig. 2. Samples were collected using the method of Emerson et al. (1995). Borosilicate glass flasks (300–500 mL) with 9 mm Louwers–Hapert valves were first triple-rinsed with deionized water. All internal valve surfaces were degreased with 2-propanol and thoroughly cleaned to remove particulate matter. The valve stems were similarly degreased, and the Viton O-rings were replaced and lubricated. To each flask, 100 μL of saturated $HgCl_2$ was added and dried at 40 °C. For the largest expected sample volume (250 mL), the $HgCl_2$ concentration is 28 μg mL^{-1}, greater than the 20 μg mL^{-1} concentration recommended by Kirkwood (1992). All flasks were then evacuated to less than 1.0×10^{-3} torr. Samples were collected by entraining bubble-free seawater from the valve side arm into the evacuated flask. Following headspace equilibration, the excess seawater was removed under vacuum and the residual seawater frozen at −55 to −60 °C in a chilled 2-propanol bath. The sample O_2 and Ar were separated from N_2, CO_2, and H_2O by an automated gas chromatographic system described by Blunier et al. (2002) (and see also Barkan and Luz, 2003), cryogenically trapping the analyte gases at $T < 20$ K. Following sample warming to 300 K and a 4 h equilibration, $\delta^{17}O$, $\delta^{18}O$, and O_2/Ar were measured by dual inlet mass spectrometry (Finnigan MAT 252). The $\delta^{17}O$ and $\delta^{18}O$ ratios were measured via multicollection, and O_2/Ar ratios were measured by peak jumping.

The external precision of the sample preparation and mass spectrometric techniques was first evaluated by replicate analyses of a dry, compressed air standard (1.8 scc aliquots). The standard was admitted to the processing line without passing through the sample manifold; the subsequent processing was identical to the samples. For 20 aliquots analyzed over 40 days, the 1σ standard deviation from the mean was ±0.02‰ ($\delta^{18}O$), ±0.03% (O_2/Ar), and ±7.3 per meg ($^{17}\Delta$). A second estimate of the overall precision comes from the standard deviation from the mean of replicate flasks analyzed from a single cruise (NBP02-09, 46 pairs). The rms deviation from the mean of replicates was ±6 per meg, ±0.35%, and ±0.08‰ for $^{17}\Delta$, O_2/Ar, and $\delta^{18}O$, respectively. These values correspond to population standard deviations of ±0.5% for O_2/Ar and ±9 per meg for $^{17}\Delta$. Since samples were almost always analyzed in duplicate, resulting standard errors for bottles filled at a single location

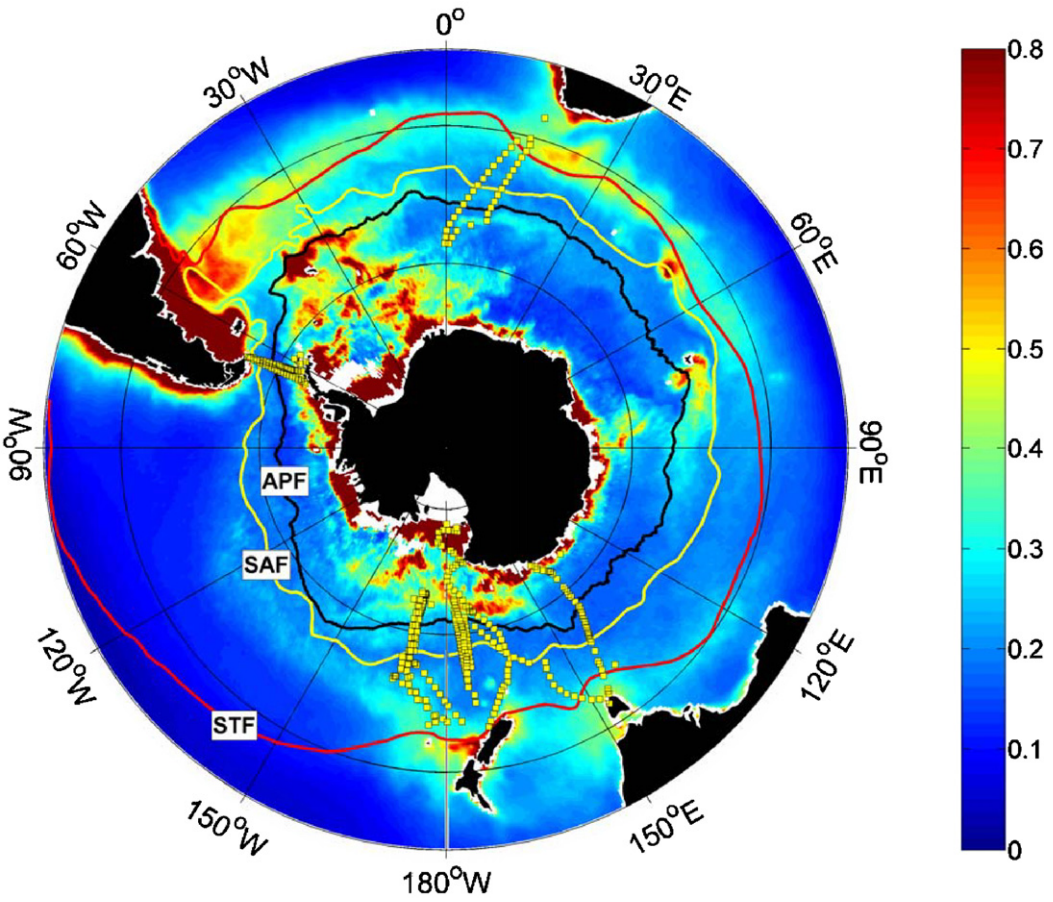

Fig. 2. Site location map for the Southern Ocean mixed layer samples, plotted as closed squares. The regions sampled in this work lie south of New Zealand, south of Australia, south of South Africa, and in the Drake Passage. Chlorophyll *a* concentrations represent mean SeaWiFS [chl-*a*] from September 1997 to October 2003 ($mg\,m^{-3}$). Data were provided by the Goddard Earth Science (GES) Distributed Active Archive Center (DAAC, http://daac.gsfc.nasa.gov). The linear color scale is truncated at $0.8\,mg\,m^{-3}$ to emphasize low and intermediate concentrations, and the original data set was coarsened five-fold prior to gridding. Note the elevated Subantarctic concentrations east of South America, southeast of South Africa, and southeast of Australia. Elevated [chl-*a*] is also observed transecting the Antarctic Circumpolar Current near the Ross and Weddell Seas. The location of the Subtropical Front (STF), Subantarctic Front (SAF), and Antarctic Polar Front (APF) follow Orsi et al. (1995). Solid circles correspond to 40°S, 60°S, and 80°S.

are $\pm 0.35\%$ for O_2/Ar, ± 6 per meg for $^{17}\Delta$, and $\pm 0.08‰$ for $\delta^{18}O$. Note that the standard deviation from the mean for $\delta^{18}O$ is greater than for $^{17}\Delta$. As stated by Hendricks et al. (2004), the errors in $\delta^{18}O$ and $\delta^{17}O$ result mainly from mass-dependent fractionation during sample processing and analysis. This mass-dependent fractionation does not introduce error into $^{17}\Delta$.

Analytical uncertainties and uncertainties in the gas exchange coefficient both contribute to errors in air–sea fluxes. When O_2/Ar and $^{17}\Delta$ values are close to equilibrium, errors arise mainly from analytical uncertainties, whereas when O_2/Ar and O_2 values are large, errors arise mainly from uncertainties in the gas exchange coefficient. Consider a typical water sample with $[O_2] = 320\,mmol\,m^{-3}$, the equilibrium values of O_2/Ar and O_2, and our ensemble mean gas exchange coefficient of $5.5\,m\,day^{-1}$. A standard error of ± 6.3 per meg in O_2 corresponds to an uncertainty of $\pm 2.6\%$ ($\pm 8.4\,\mu mol/L$) in the inventory of photosynthetic O_2, given an anomaly of 249 per meg in the triple isotope composition of air O_2. This uncertainty leads to an uncertainty in gross photosynthetic O_2 production of $\pm 46\,mmol\,m^{-2}\,day^{-1}$. Similarly, a standard error in O_2/Ar of $\pm 0.35\%$ corresponds to an uncertainty of $\pm 1.1\,mmol\,m^{-3}$ in the biological O_2 supersaturation, and an uncertainly of $6.2\,mmol\,m^{-2}\,day^{-1}$ in

Table 2
Southern Ocean transits included in this study

Sampling group and affiliation	Research vessel	Cruise	Symbol	Start date	End date	Transects	Location
S. Jacobs, LDEO	RVIB *Nathaniel B. Palmer*	2000-01	NBP0001	3/25/2000	3/29/2000	1	Drake Passage
J. Wieland, SIO	R/V *Yuzhmoregeologiya*	AMLR-2002	AMLR02	1/17/2002	1/29/2002	1	Drake Passage
C. Frohlich and F. Taylor, UTIG	ASRV *Laurence M. Gould*	2002-09	LMG0209	11/25/2002	12/22/2002	2	Drake Passage
H. Ducklow, VIMS	ASRV *Laurence M. Gould*	2003-01	LMG0301	2/5/2003	2/6/2003	1	Drake Passage
H. Ducklow, VIMS	ASRV *Laurence M. Gould*	2004-01	LMG0401	1/3/2004	2/4/2004	2	Drake Passage
S. Jacobs, LDEO	RVIB *Nathaniel B. Palmer*	2000-08	NBP0008	12/21/2000	1/23/2001	2	South of Australia
T. Trull, U. Tasmania	R/V *Aurora Australis*	2001-03	A0103	10/30/2001	12/10/2001	2	South of Australia
J. Maisano, USCG	USCG *Polar Star*	2003-01	PSTAR03	12/14/2003	12/19/2003	1	South of Australia
D. Caron, USC	RVIB *Nathaniel B. Palmer*	1999-01	NBP9901	12/21/1999	2/8/2000	1	South of New Zealand
M. Gorbunov, Rutgers	R/V *Melville*	SOFEX-2002	SOFEXM	1/20/2002	2/24/2002	2	South of New Zealand
S. Tozzi, Rutgers	R/V *Revelle*	SOFEX-2002	SOFEXR	1/7/2002	2/12/2002	2	South of New Zealand
M. Reuer, Princeton	RVIB *Nathaniel B. Palmer*	2002-09	NBP0209	12/12/2002	12/31/2002	1	South of New Zealand
P. Neale, SERC	RVIB *Nathaniel B. Palmer*	2003-05	NBP0305	10/28/2003	11/13/2003	2	South of New Zealand
W. Smith, VIMS	RVIB *Nathaniel B. Palmer*	2003-05A	NBP0305A	12/20/2003	12/29/2003	1	South of New Zealand
T. Brey and K. Beyer, AWI	R/V *Polarstern*	ANTXXI/2	ANTXXI/2	11/18/2003	1/15/2004	2	South of South Africa

Note that mixed layer samples were collected from four principal regions, and most transits were completed during the austral summer.

the air–sea O_2 flux. On the other hand, when O_2 and O_2/Ar ratios are far from equilibrium, the main source of error comes from the gas exchange coefficient. The error reported for the quadratic parameterization of Wanninkhof (1992) is $2.2\,m\,day^{-1}$. Given our average gas exchange coefficient of $5.5\,m\,day^{-1}$, the uncertainty in flux due to gas exchange is 40%. With respect to net/gross estimates, uncertainties in O_2/Ar and O_2 translate to errors that are small when disequilibrium is large, and approach infinity as disequilibrium goes to zero. The best uncertainty estimates for net/gross O_2 production come from the standard errors of averages by zone and cruise. These are included in Fig. 6.

Because uncertainties are large, we focus on trends in the data and aggregated results rather than numbers for individual stations. Given typical sampling frequencies, we generally collect 5–10 samples per cruise in each oceanographic zone. If one regards uncertainties as Gaussian (valid for analytical uncertainties but not necessarily for those associated with windspeed), then standard errors in average fluxes are a factor of ~2–3 less than numbers in the previous paragraph.

3.1. Determination of the air–water $^{17}\Delta$ disequilibrium

In this study, we determined $^{17}\Delta_{eq}$, the $^{17}\Delta$ difference between dissolved O_2 and air O_2 at equilibrium. A 35 psu NaCl solution was placed into a 4000 mL beaker, poisoned with $20\,\mu g\,mL^{-1}$ [$HgCl_2$], and continuously stirred with a magnetic

stir bar. Throughout the experiment the dissolved [O_2] was monitored by an oxygen optode (Aanderaa Instruments), and a constant optode reading ($\pm 0.2\,\mu mol\,L^{-1}$ over 5.3 h, 1σ standard deviation) was observed within 12 h at either 11 °C or 25 °C. After this time, O_2/Ar was measured and found to be within ± 3‰ of the equilibrium value. After 24–48 h, 150 mL samples were collected into evacuated glass flasks, equilibrated by rotation for 12 h, and processed according to the method described above.

The $^{17}\Delta_{eq}$ result requires accurate measurements of the zero enrichment, which is the isotopic difference measured when the same gas is admitted to the sample and reference inlets of the mass spectrometer. Accurate standard corrections are also required. For this experiment, 17 measurements of the zero enrichment, 13 measurements of air O_2, and 30 measurements of the dissolved $^{17}\Delta$ were completed. Fifteen water replicates were measured at 25 °C and fifteen at 11 °C, and the results are shown in Fig. 3. Differences between the measured $\delta^{18}O$ values for the two experiments agree well with the expected values from the Benson and Krause (1984) solubility relationship (Fig. 3). Thus, the measured $^{17}\Delta$ values reflect near-equilibrium conditions. The $^{17}\Delta$ results show no significant difference between the two temperatures, and the mean value (8 ± 11 per meg, 1σ, $n = 30$, corresponding to a standard error of ± 2 per meg) is less than the Luz and Barkan (2000) estimate (16 per meg). This lower $^{17}\Delta_{eq}$ value of 8 per meg is appealing because it provides a λ value (as defined by Eq. (4)) of 0.528, approximately the value expected for equilibrium processes. In this study we adopt a $^{17}\Delta_{eq}$ value of 8 per meg. This reduction increases the gross oxygen production estimates and lowers the N/G production values.

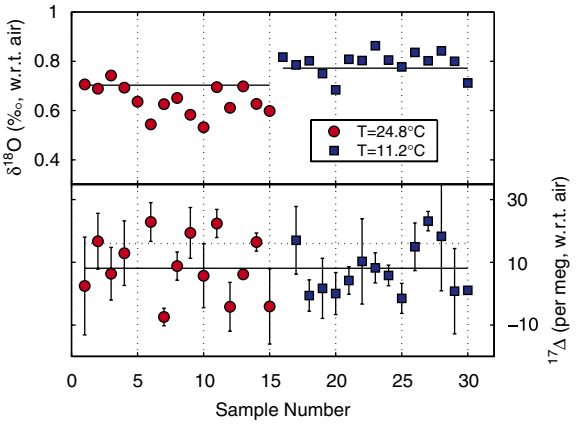

Fig. 3. Results of the experiment to determine equilibrium $^{17}\Delta$ fractionation between gaseous and dissolved O_2 at 11.2 and 24.8 °C. Upper panel, $\delta^{18}O$ of dissolved O_2; lower panel, $^{17}\Delta$. Lower panel shows the $^{17}\Delta$ results. The equilibrium $^{17}\Delta_{eq}$ value of +0.016‰, measured by Luz and Barkan (2000, 16 per meg, dotted line) and $^{17}\Delta_{eq}$ observed here for both temperatures (8 per meg) is represented by the solid line. Error bars are $\pm 1\sigma$ standard error of replicate mass spec analyses ($n = 3$ blocks of 30 cycles). The mass spectrometer errors in $\delta^{18}O$ are smaller than the plotted symbols, but the chromatographic separation and sample handling introduce additional errors.

3.2. Gas permeation and sample contamination

Permeation of O_2 and Ar through Viton O-rings warrants consideration given Southern Ocean sampling logistics. This problem has been discussed by Sturm et al. (2004) for atmospheric O_2/N_2 measurements and multiple elastomers. For a single Viton O-ring (area = 0.27 cm^2, thickness = 0.14 cm) and a 0.209 atm pO_2 gradient, the expected leak rate is 6.4 $\mu mol\,O_2\,yr^{-1}$ if one assumes a permeability coefficient of 1.1×10^{-11} cc cm $cm^{-2}\,s^{-1}\,hPa^{-1}$ (Ma et al., 1995). Such a leak rate is problematic for our samples, given their [O_2] of ~300 $\mu mol\,L^{-1}$, 0.25 L sample volumes, and storage periods of about 4–7 months (from precruise evacuation to analysis). Therefore, we performed the permeability experiments under conditions appropriate to our samples.

To measure the leak rate for O_2 and Ar, 9 mm internal diameter Louwers–Hapert valves were utilized, containing a cylindrical shaft and a valve stem with three Viton O-rings (see Fig. 1a of Sturm et al., 2004). The glass tube isolated by the valve was flame sealed, evacuated to less than 5×10^{-4} torr, and sealed with the normal terminal Viton O-ring. Following evacuation, the side arms of some tubes were filled with deionized water, which is how we store our samples. Other tubes were simply exposed to air. Tubes were allowed to sit for up to 256 days. Oxygen and argon concentrations were determined on a ThermoFinnigan DeltaPlus dual inlet mass spectrometer. We determined the sensitivity at each mass using a gas standard admitted to a calibrated volume with pressures characterized with a differential pressure gauge (MKS Barotron, 0–100 torr) referenced to a laboratory barometer (Princo Instruments). The results for 7, 47, and 256 days are shown in Table 3. First, oxygen permeation rates were consistently lower for the "wet" O-rings exposed to deionized water. The seven-day experiment produced O_2 leak rates of 10.1 $\mu mol\,yr^{-1}$ (dry)

Table 3
Leak experiments for Louwers–Hapert valves fitted with Viton O-rings

Valve arm condition	Duration (days)	Mean O_2 leak rate (umol/yr)	Mean O2/Ar (corrected)
Air-filled valve	7	10.1 ± 2.1 ($n = 2$)	17.2 ± 0.3 ($n = 2$)
	256	3.4 ± 1.2 ($n = 2$)	15.7 ± 2.3 ($n = 2$)
Water-filled valve	7	2.9 ± 0.4 ($n = 2$)	22.6 ± 0.1 ($n = 2$)
	47	1.4 ± 0.3 ($n = 3$)	22.6 ± 3.3 ($n = 3$)
	256	0.8 ± 0.2 ($n = 3$)	32.4 ± 8.3 ($n = 3$)

Note the significant reduction in the O_2 leak rate versus time and the reduced leak rates for the water-filled valves. The elevated O_2/Ar ratio observed on day 256 was significantly higher than the previous two observations despite equivalent analytical conditions.

Table 4
Averages for gross O_2 production, net O_2 production, and the N/G ratio calculated from data in physical oceanographic zones of the Southern Ocean on individual transits

Cruise	Start date	End date	Location	Gross O_2 prod.			Net O_2 prod.			N/G ratio		
				SAZ	PFZ	AZ	SAZ	PFZ	AZ	SAZ	PFZ	AZ
NBP0001 (S)	3/25/2000	3/29/2000	Drake Passage			114			−2			−0.02
LMG0209 (S)	11/25/2002	11/29/2002	Drake Passage		61	32		21	3		0.34	0.11
LMG0209 (N)	11/29/2002	12/22/2002	Drake Passage		150	57		22	9		0.14	0.16
LMG0301 (S)	2/5/2003	2/6/2003	Drake Passage		52	23		5	−4		0.09	−0.17
LMG0401 (S)	1/3/2004	1/26/2004	Drake Passage			46			−2			−0.04
LMG0401 (N)	1/27/2004	2/4/2004	Drake Passage		95	114		27	11		0.29	0.09
NBP0008 (S)	12/21/2000	1/16/2001	South of Australia	491	382	98	61	23	8	0.12	0.06	0.09
NBP0008 (N)	1/18/2001	1/23/2001	South of Australia	321	284	122	53	34	17	0.16	0.12	0.14
A0103 (S)	10/30/2001	11/29/2001	South of Australia		113			29			0.25	
A0103 (N)	12/4/2001	12/10/2001	South of Australia	472	212	233	73	30	29	0.15	0.14	0.12
PSTAR03 (S)	12/14/2003	12/19/2003	South of Australia	295	135	40	22	36	14	0.07	0.27	0.35
NBP9901 (S)	12/21/1999	2/8/2000	South of New Zealand	293	271	179	14	4	18	0.05	0.01	0.10
SOFEXM (S)	1/20/2002	2/3/2002	South of New Zealand	347		160	35		6	0.10		0.03
SOFEXM (N)	2/16/2002	2/24/2002	South of New Zealand	206	254	209	34	27	19	0.17	0.11	0.09
SOFEXR (S)	1/7/2002	1/23/2002	South of New Zealand	206	137	110	32	13	−3	0.15	0.10	−0.02
SOFEXR (N)	2/5/2002	2/12/2002	South of New Zealand	172	133	127	29	13	19	0.17	0.10	0.15
NBP0209 (S)	12/12/2002	12/31/2002	South of New Zealand	260	193	108	61	30	19	0.23	0.16	0.17
NBP0305 (S)	10/28/2003	11/13/2003	South of New Zealand		258	156		40	26		0.15	0.17
NBP0305 (N)	11/13/2003	11/16/2003	South of New Zealand	352	286	181	48	13	9	0.14	0.05	0.05
NBP0305A (S)	12/20/2003	12/29/2003	South of New Zealand		214	77		17	35		0.08	0.46
			Mean Drake Passage		89	64		19	3		0.22	0.02
			Mean South of Australia	395	225	123	52	30	17	0.13	0.17	0.18
			Mean South of New Zealand	262	218	145	36	20	16	0.14	0.09	0.13

All flux estimates are given in mmol m^{-2} day^{-1}. The cruise abbreviations are given in Table 2, and southbound (S) and northbound (N) transits are denoted. We do not include samples collected in the Bransfield Strait and south of Africa in this compilation. The African sector is represented by only two transects; as in other regions, rates tend to be higher in the north.

and 2.9 μmol yr^{-1} (wet). Second, the O_2/Ar ratios were also significantly different for dry and wet conditions: the dry results were slightly less than the seawater saturation ratios of ~20.5 (17.2 ± 0.3 after 7 days), whereas the wet results were slightly higher (22.6 ± 0.1 after 7 days). Finally, the time-averaged permeation rates with water seals diminished throughout the experiment, decreasing from 2.9 ± 0.4 μmol yr^{-1} at 7 days to 0.8 ± 0.2 μmol yr^{-1} at 256 days.

Given these data, how much will permeation affect the O_2/Ar ratio? If one assumes a power-law reduction in the O_2 leak rate with time, an O_2/Ar permeation ratio of 22.6, and a characteristic

Subantarctic water sample ($V = 250$ mL, $T = 10$ °C, $S = 34.5$ psu, $P = 996$ hPa), the associated error in the O_2/Ar ratio equals 0.10% after 6 months, and 0.16% after 1 year. These estimates are likely lower limits given elevated O_2/Ar ratios permeating the Viton seals; ratios reaching 32 were observed for the water-filled experiments (Table 3). The observed sample uncertainty ($\pm 0.5\%$) is larger, probably because of uncertainties introduced during sample collection and processing. In any case, the time between the final flask evacuation and sample analysis was minimized, typically 6 months and almost always less than 12 months.[3] As suggested by Sturm et al. (2004), the use of different valve types (e.g., conical valve seals), less permeable elastomers (Kel-F), or reduced evacuation-to-analysis periods could significantly reduce this uncertainty.

Finally, we note that leakage has a completely negligible effect on the isotopic composition of O_2.

4. Results and discussion

The $^{17}\Delta$ and $\Delta(O_2/Ar)$ observations offer new high-resolution estimates of net and gross production within the Southern Ocean mixed layer. Individual sample results from each cruise are given in the online version of this paper. We first discuss the rates of gross O_2 production and compare them with satellite productivity estimates. The net O_2 production rates and the export/gross ratios are then presented. We calculate average rates of gross O_2 production, net O_2 production, and the net/gross ratio for each zone and transit (Table 4). The ensuing discussion includes comparisons between our data and other measures of production.

We emphasize that exact agreement among the various productivity estimates cannot be expected. Data from the different approaches reflect different scales of time and space. Our results do not include production below the mixed layer, and they have significant uncertainties associated with the gas exchange parameterization and analytical error (especially for gross production). All other flux estimates have their own uncertainties. However, meaningful comparison is possible among the tracer results, bottle incubation data, and satellite productivity estimates.

[3]The 6-month period between flask evacuation and analysis was due to shipping constraints, not analytical throughput.

4.1. Gross O_2 production rates: spatial variability and comparison with satellite estimates

Mixed layer $^{17}\Delta$ and gross O_2 production versus latitude are shown in Figs. 4 and 5, including separate panels for each cruise. Nearly all $^{17}\Delta$ observations are greater than the equilibrium $^{17}\Delta$ value (8 per meg), reflecting the presence of O_2 produced in situ by photosynthesis. Gross O_2 production is determined from the measured $^{17}\Delta$ value relative to equilibrium and the gas exchange coefficient. The corresponding Vertically Generalized Productivity Model (VGPM) results of Behrenfeld and Falkowski (1997) are also plotted. This productivity algorithm reflects ^{14}C primary productivity calculated from surface chlorophyll *a* concentration ([chl-*a*]), SST, and photosynthetically active radiation (PAR).

Two primary trends are apparent in our gross O_2 production data. First, gross O_2 production is higher in the western Pacific sector of the Southern Ocean than across the Drake Passage. This result is expected from ocean color observations. Mean annual SeaWiFS [chl-*a*] in Fig. 2 is consistently lower in the Drake Passage, with elevated [chl-*a*] along its southern and northern margins (South Shetland Islands and Straits of Le Maire). Second, gross O_2 production is often highest at the northern margins of the transits (Table 5). This pattern was observed for all four transits south of Australia. South of New Zealand, this pattern holds for all six cruises except NBP9901. In the Drake Passage, it is true for both transits of LMG0209. The meridional gradient is also observed during the R/V *Polarstern* cruise south of Africa (PSTN03). In most cases VGPM also rises to the north, partially reflecting increased [chl-*a*] as determined by ocean color observations (Fig. 2). The northward increase in GPP is also shown in Fig. 6, where regionally aggregated gross O_2 production rates for each transit are plotted versus net O_2 production rates. On average, gross production rates are highest in the Subantarctic Zone, lower in the Polar Frontal Zone, and lowest in the Antarctic Zone (Table 4). In both panels of Fig. 6, there is less scatter in net/gross ratios when rates are higher or anomalies with respect to the saturation values are higher. This trend reflects the fact that samples with small anomalies have the same absolute uncertainties as larger anomalies, but uncertainties relative to the saturation values are larger.

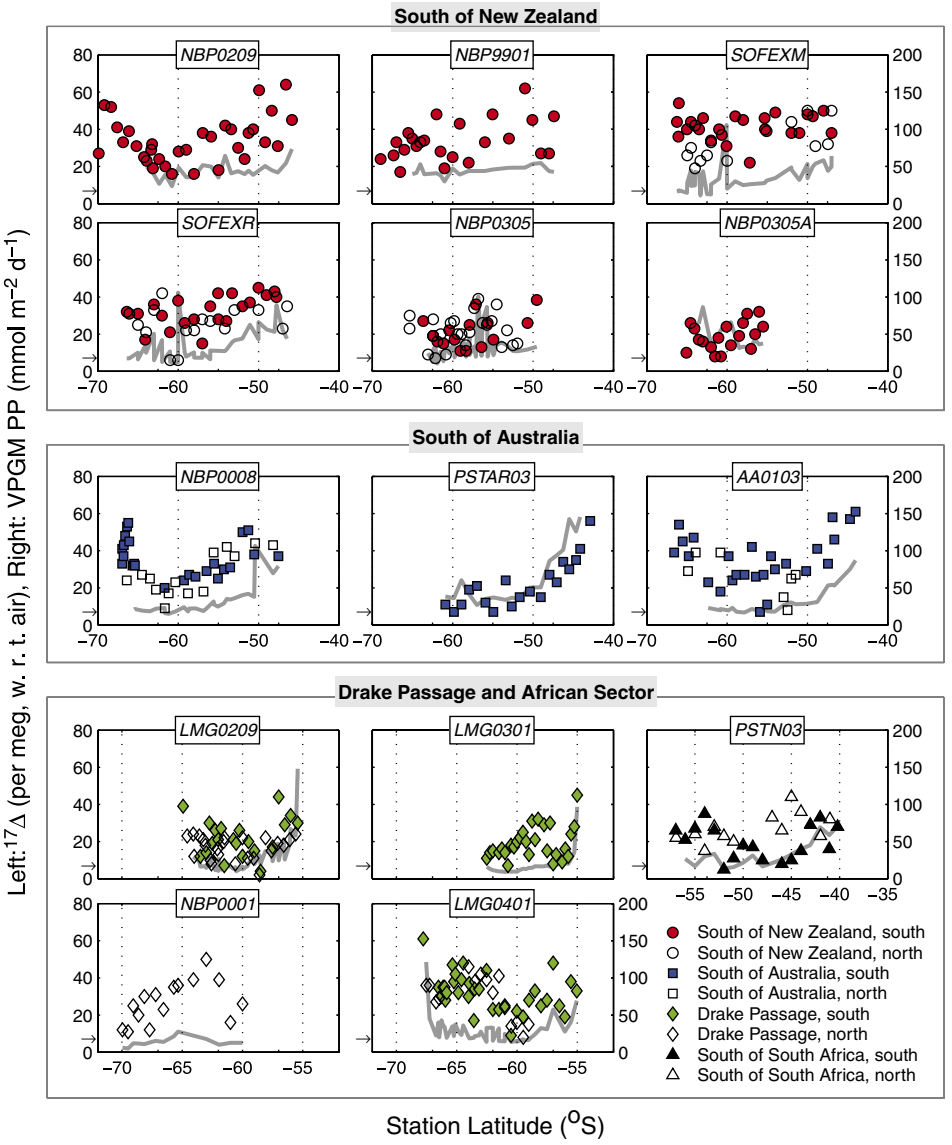

Fig. 4. Southern Ocean mixed layer $^{17}\Delta$ vs. latitude. The left axes and symbols show the oxygen triple isotope composition, calculated in per meg units with respect to air. The arrow on the left axis indicates the assumed equilibrium $^{17}\Delta$ value associated with air–sea gas exchange (8 per meg). The right axes and solid lines reflect ^{14}C productivity estimates from Behrenfeld and Falkowski (1997). Closed symbols denote southbound transits, and open symbols reflect northbound transits. All cruise abbreviations are defined in Table 2. We exclude Marginal Ice Zone samples from these transect plots. As discussed in the Experimental Methods section, the best estimate for the $^{17}\Delta$ uncertainty is ± 9 per meg (1σ).

Our results provide a large, self-consistent database to test satellite-based primary productivity estimates. We limit this comparison to the VGPM, primary production as computed by the Behrenfeld and Falkowski (1997) model, based on SeaWiFS version 4 estimates of ocean chlorophyll. In the comparison we include shipboard productivity based on ^{14}C and ^{18}O labeling experiments carried out during the US JGOFS Southern Ocean program along 170°W (Dickson and Orchardo, 2001; Hiscock et al., 2003). This comparison is of interest since the incubation data were not included in the original model calibration, which is dominated by subtropical and equatorial stations. ^{14}C and ^{18}O productivity values were integrated to the 1% light level and are thus directly comparable to VGPM,

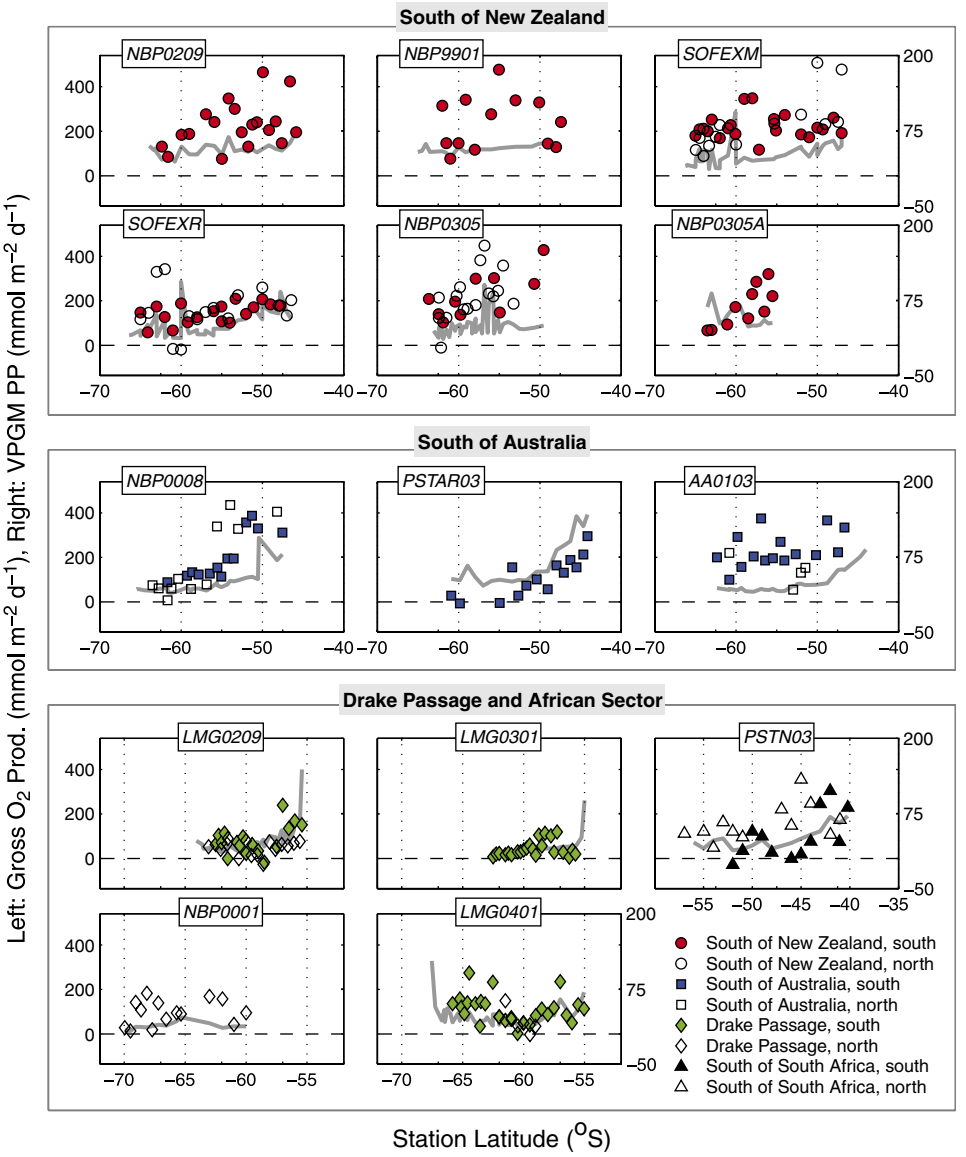

Fig. 5. Southern Ocean mixed layer gross O_2 production vs. latitude. The left axes and symbols show gross O_2 production rates in mmol m^{-2} d^{-1}. The right axes and solid lines reflect ^{14}C productivity estimates from Behrenfeld and Falkowski (1997), as in Fig. 4. Closed symbols denote southbound transits, and open symbols reflect northbound transits. All cruise abbreviations are defined in Table 2.

which is intended to represent the ^{14}C productivities integrated to this horizon. GPP values of this study, based on mixed layer $^{17}\Delta$ values, access only the mixed layer. However, results from the US JGOFS Southern Ocean experiment (for example) indicate that productivity is low below the (relatively deep) Southern Ocean mixed layer (http://usjgofs.whoi.edu/jg/dir/jgofs/southern/).

Depth-integrated ^{14}C and ^{18}O productivity values from the JGOFS dataset are plotted versus VGPM ^{14}C primary productivity in Fig. 7. All ^{14}C primary productivity results (including VGPM) were converted to gross O_2 fluxes by assuming a 2.7 conversion factor, reflecting the ratio of gross O_2 production to ^{14}C production measured in a series of bottle intercomparison experiments (Marra, 2002). Thus we expect that O_2 GPP values plotted versus ^{14}C primary productivity should fall on a line with a slope of 2.7. Where satellite primary productivity estimates are less than 30 mmol m^{-2} d^{-1}, the bottle incubation estimates are in excellent agreement with VGPM. Above

Table 5
Comparison of new, net, and export production estimates for the austral summer mixed layer along 170°W

Zone	Latitude	Net prod. ($\Delta O_2/Ar$)) [this study]	New prod. ($^{15}NO_3^-$) [2]	POC flux (^{234}Th) [3]	Modeled POC Flux [4]	Seasonal ΔNO_3 [5]	Seasonal ΔpCO_2 [6]	$\Delta[O_2]$, in vitro [7]
SAZ	46–55°S	36	30	10	19	x	x	90
PFZ	55–60°S	20	12	10	19	18	25	14
AZ	60–64°S	16	29	15	14	25	29	44

All rates are expressed as mmol C m^{-2} day^{-1}. The citations include: (1) net production rates from this study, inferred from $\Delta(O_2/Ar)$; (2) Sambrotto and Mace (2000); (3) Buesseler et al. (2001); (4) Schlitzer (2002); (5) Lourey and Trull (2002); (6) Morrison et al. (2001); and (7) Dickson and Orchardo (2001). The Dickson and Orchardo (2001) results are from in vitro $\Delta[O_2]$ measurements. The modeled POC fluxes from Schlitzer (2002) were converted from his Fig. 5 and assume a growing season of 120 days. They should be considered approximate. Note the general agreement between $\Delta(O_2/Ar)$ and ^{15}N within the Subantarctic and Polar Frontal Zones and the lower $\Delta(O_2/Ar)$ estimates within the Antarctic Zones.

30 mmol m^{-2} d^{-1} the ^{14}C and ^{18}O incubation results fall above the expected line, but only by about 40%. Our aggregated $^{17}\Delta$ productivity estimates scatter about a line with twice the expected slope ($m = 5.4$). The scatter itself is approximately a factor of 2, typical for productivity data-model intercomparisons. Both the $^{17}\Delta$ productivity measurements and the bottle incubation results thus suggest that the Behrenfeld and Falkowski (1997) algorithm sometimes underestimates primary production in the study region. The new bottle data are generally supportive of VGPM, while suggesting a possible improvement at higher productivities. The $^{17}\Delta$ data suggest that VGPM systematically underestimates ^{14}C production by about a factor of 2. An alternative explanation for the comparison between $^{17}\Delta$ and ^{14}C rates is that there is extensive O_2 cycling in the Southern Ocean, by the Mehler Reaction or chlororespiration, which proceeds without fixation of CO_2.

4.2. Magnitude and variability of net O_2 production rates

As shown in Figs. 6 and 8, O_2/Ar ratios are almost always above the saturation value, signifying that the austral summer mixed layer is generally net autotrophic. Negative values were occasionally observed in the Antarctic Zone, and the implied negative net O_2 production rates warrant consideration. Enhanced upwelling occurs within the Polar Frontal Zone (PFZ) and Antarctic Zone (AZ) given the elevated wind stress curl. Upwelling brings O_2-undersaturated waters into the mixed layer, leading us to underestimate NCP. Seasonal 1-dimensional model estimates of Wang et al. (2001) show comparable vertical P fluxes during the December–January–February (DJF) season in the Subantarctic (1.2 mmol m^{-2}, comparable to 7% of P export) and Polar Frontal Zone (2.5 mmol m^{-2}, comparable to 10% of P export). According to their calculations, ~20% of P resupply within the DJF Polar Frontal Zone results from vertical mixing compared to horizontal advection (2.5 versus 12.3 mmol m^{-2}), suggesting that vertical fluxes play a small role in the biogeochemical mass balance once the growing season is underway (see Table 2 of Wang et al., 2001). The situation is most problematic in the Marginal Ice Zone south of New Zealand. Here, biological O_2 undersaturation reaches −14% at 77°S, 178°W (December 2002), and modeling results of Wang et al. (2001) suggest that vertical mixing is more important. We attribute O_2 undersaturation in the Marginal Ice Zone to vertical mixing rather than net heterotrophy, and net O_2 production estimates must generally be interpreted with caution near the ice margin and within the southern Antarctic Zone. We assume that waters with biological O_2 undersaturation below −0.5% are undersaturated due to upwelling and exclude them from calculations of net O_2 production (Tables 4–6, Figs. 6–7). All other samples are included in our tabulations. However, even O_2-supersaturated samples in the Antarctic Zone may be influenced by upwelling, and NCP in this zone may be greater than we calculate. The effect of upwelling on gross production is considerably smaller, because upwelling does not lower $^{17}\Delta$ values below atmospheric equilibrium (Hendricks et al., 2004).

The spatial variability in net O_2 production is similar to gross O_2 production. However, the relative analytical uncertainties for $\Delta(O_2/Ar)$ are smaller than $^{17}\Delta$, and the geographic variability is more clearly expressed. The mixed layer $\Delta(O_2/Ar)$

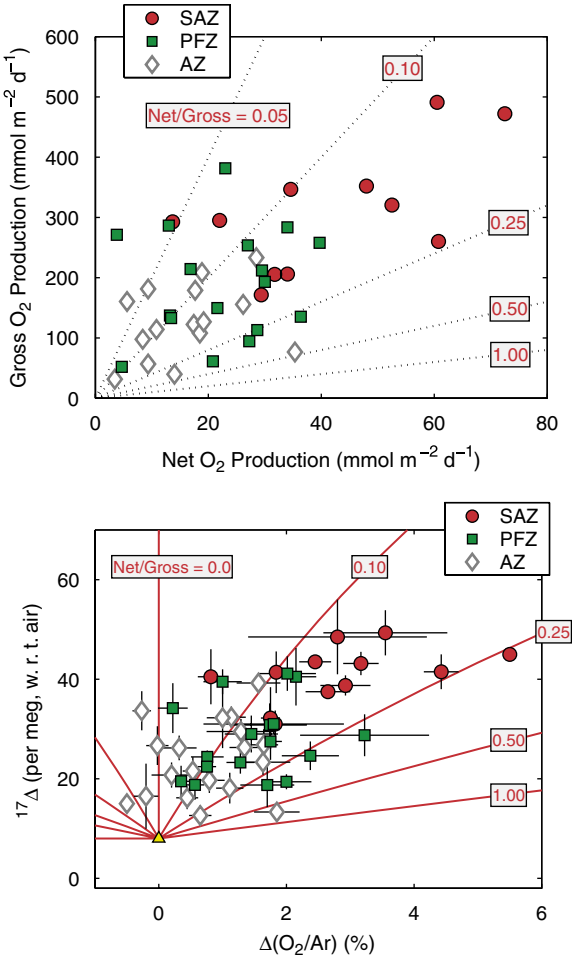

Fig. 6. *Upper panel*: gross vs. net community O_2 production in the mixed layer, and the corresponding N/G ratios. *Lower panel*: $^{17}\Delta$ (a measure of gross O_2 production) vs. biological O_2 saturation (a measure of net O_2 production). Each point represents the average of all data collected within a single zone on one transit across the Southern Ocean, including the Subantarctic Zone (SAZ), the Polar Frontal Zone (PFZ), and the Antarctic Zone (AZ). Error bars in the lower panel correspond to ± 1 standard error of the mean. Superimposed are isolines of constant net/gross production. The data distribution between the upper and lower panels is not equal as the upper panel includes the gas transfer velocity parameterization.

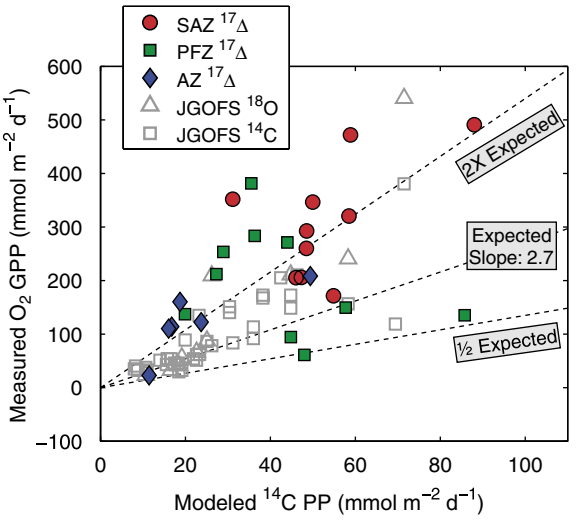

Fig. 7. Comparison of gross O_2 production rates from $^{17}\Delta$ and ^{14}C productivity from Behrenfeld and Falkowski (1997). Plotted are ^{14}C productivities along 170°W (Hiscock et al., 2003), scaled to gross O_2 production by multiplying by 2.7 (Marra, 2002); gross O_2 production along 170°W measured in vitro using ^{18}O labeling (Dickson and Orchardo, 2001); and production determined in this study with $^{17}\Delta$ of O_2. All samples with $\Delta(O_2/Ar) < -0.5\%$ were excluded from this comparison. Abbreviations follow Fig. 6.

results and associated net O_2 production estimates are shown in Figs. 8 and 9 along with the ^{14}C productivity estimates from the VGPM (Behrenfeld and Falkowski, 1997). Most of the variance in net O_2 production is determined by the $\Delta(O_2/Ar)$ results rather than the gas transfer velocity estimates, so that meridional gradients in net O_2 production are similar to $\Delta(O_2/Ar)$. For the observations south of New Zealand, a primary feature of six transits is a meridional trend in net O_2 production, with increasing values to the north. This pattern was observed on cruises spanning the growing season (November to February, cruises NBP0305, NBP0209, SOFEXM, and SOFEXR). No significant net O_2 gradient was observed in December 1999 (NBP9901) or November 2003 (NBP0305), suggesting interannual and areal variability south of New Zealand. A northward increase in NCP was also observed south of Australia. Here, between November and January, the highest NCP rates were consistently observed in the Subantarctic Zone (Fig. 9). Finally, net O_2 production within the Drake Passage and African Sector were generally lower than the other regions. On cruises LMG0209 and LMG0401, NCP rates rose to the north. Other Drake Passage cruises showed no persistent meridional trend. O_2 undersaturation was common in these waters, and we do not know whether it reflects recent upwelling or net heterotrophy (see above).

To examine seasonality in the meridional NCP gradient, we plot net O_2 production rates versus latitude in monthly bins (Fig. 10). For consistency we show only transits south of New Zealand, where we have the most data. One November transit (NBP0305) shows a maximum in production reaching 85 mmol m^{-2} d^{-1} within the Polar Frontal Zone. No Subantarctic samples were collected on this

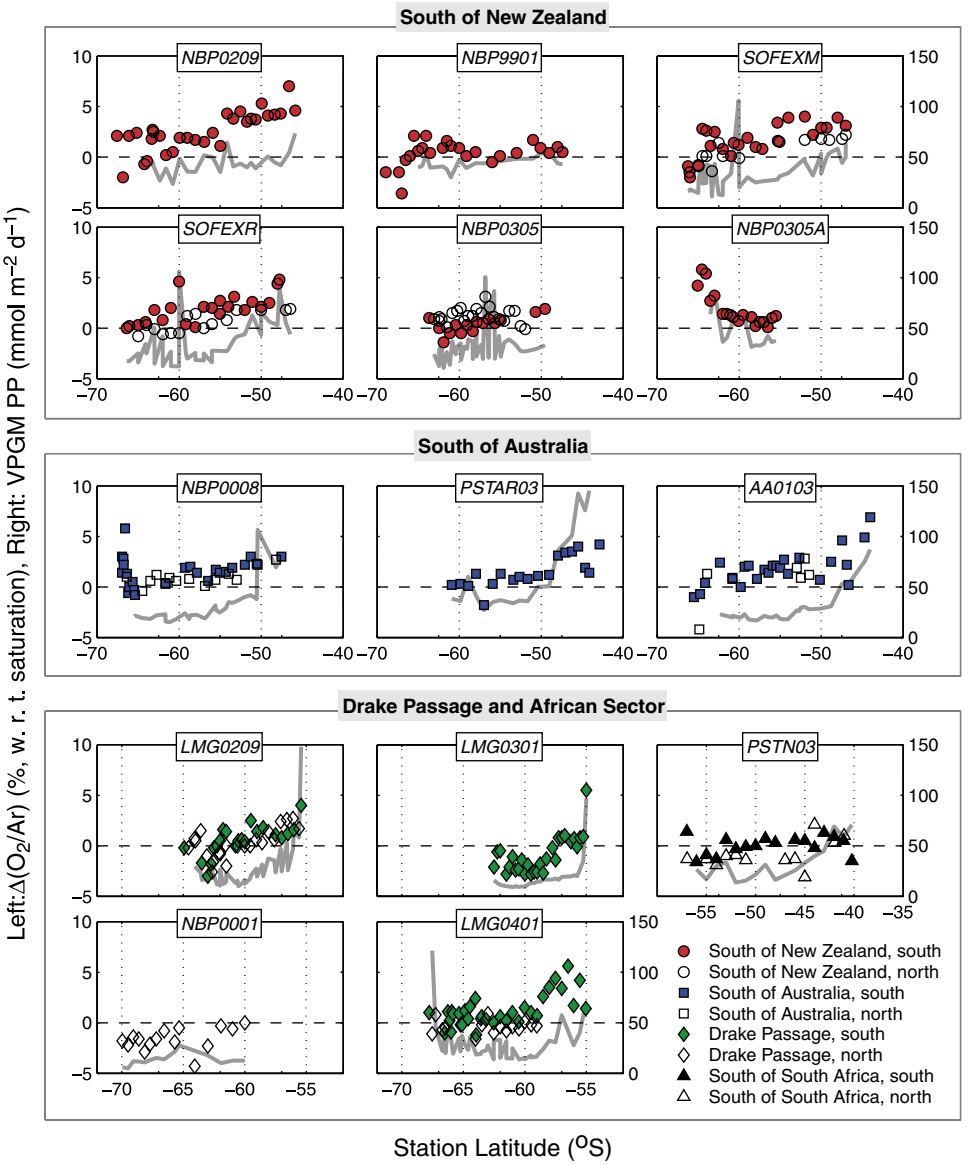

Fig. 8. Southern Ocean mixed layer $\Delta(O_2/Ar)$ observations. The left axes and symbols show the $\Delta(O_2/Ar)$ values as the percent departure from saturation. The right axes and solid lines reflect the ^{14}C productivity estimates from the Behrenfeld and Falkowski (1997) Vertically Generalized Productivity Model (units of mmol m^{-2} day^{-1}). Closed symbols denote southbound transits, and open symbols reflect northbound transits. All cruise abbreviations are defined in Table 2.

transit. A repeat November transit shows maximum values within the Subantarctic (38 mmol m^{-2} d^{-1}). The latter pattern, with NCP increasing to the north, is then observed throughout the following 3 months. The December observations show a clear transition within the Polar Frontal Zone, where net O_2 production increases from 15 mmol m^{-2} d^{-1} (55°S) to 65 mmol m^{-2} d^{-1} (54°S). These mixed layer results also suggest that spatial and interannual variability is of equal magnitude to the seasonal productivity cycle. In this limited time series south of New Zealand, the highest net O_2 production rates were observed within the Subantarctic Zone during December 2002.

We compare our net O_2 production results with other estimates of new, net, and export production, starting with our austral summer results south of New Zealand. The net O_2 results are compared to observations collected along 170°W during the US JGOFS program. These rates were compiled by

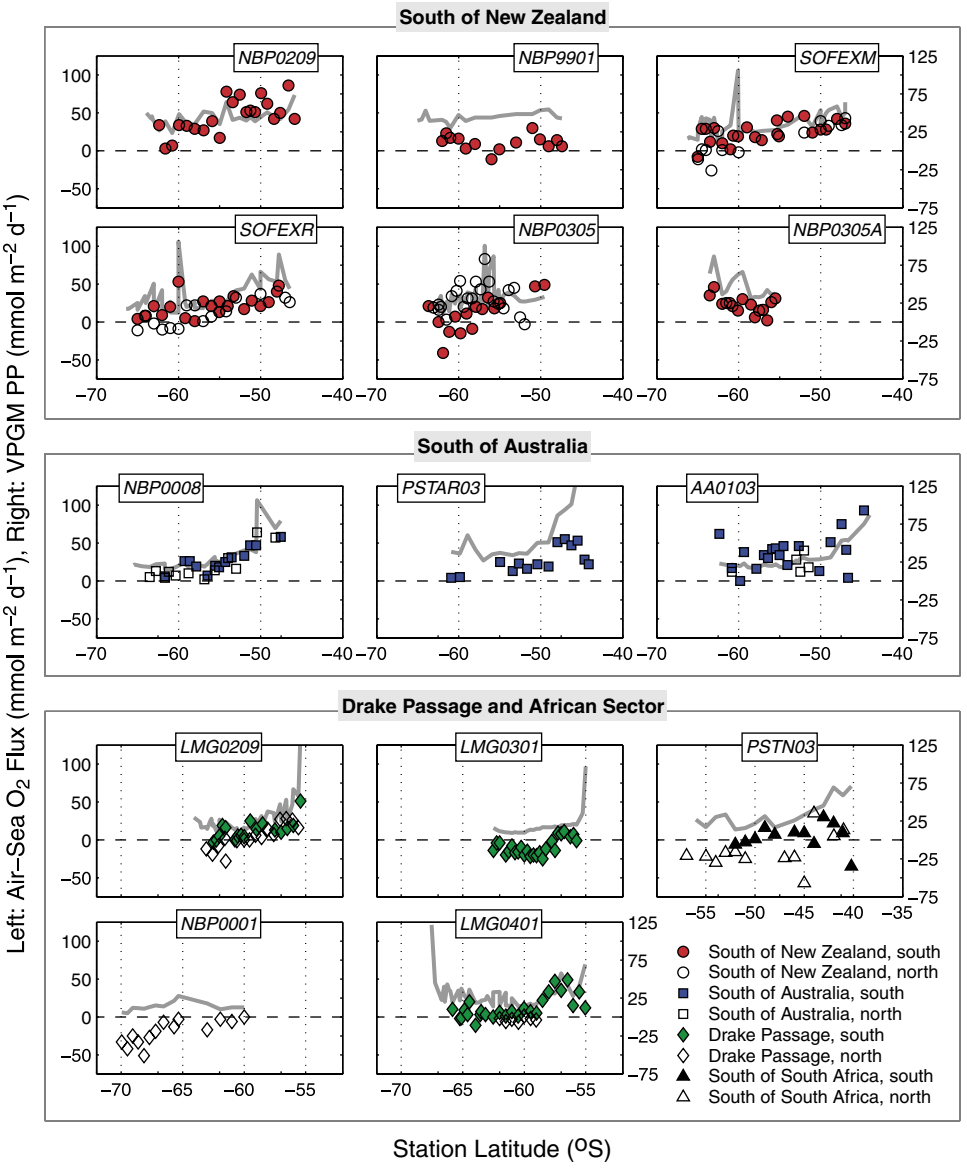

Fig. 9. Southern Ocean mixed layer net O_2 production estimates. The left axes and symbols show the calculated net O_2 production rates in mmol m^{-2} d^{-1}. The right axes and solid lines reflect ^{14}C productivity estimates from Behrenfeld and Falkowski (1997). Closed symbols denote southbound transits, and open symbols reflect northbound transits. All cruise abbreviations are defined in Table 2.

Buesseler et al. (2003), based on station data collected from December 1997 to March 1998 (see their Table 2). Their rates of new, net, and export production were determined using the following techniques: (1) net O_2 production was determined from the change in dissolved [O_2] within light/dark bottles incubated at predetermined light levels and scaled to net C production with a photosynthetic quotient of 1.4 (Dickson and Orchardo, 2001); (2) new production was determined by the ^{15}N incubation method discussed below (Sambrotto and Mace, 2000); and (3) export production at 100 m was calculated from ^{234}Th fluxes and measured values of the POC/^{234}Th ratio (Buesseler et al., 2001). We also consider modeled POC fluxes from an inverse calculation in which nutrient distributions constrain carbon fluxes (Schlitzer, 2002) and NCP estimates from seasonal NO_3 and pCO_2 drawdown (Morrison et al., 2001; Nelson et al., 2002). For consistency all estimates have been grouped into the three zones presented here (Subantarctic Zone, Polar Frontal Zone, and Antarctic Zone). Results are shown in Table 5.

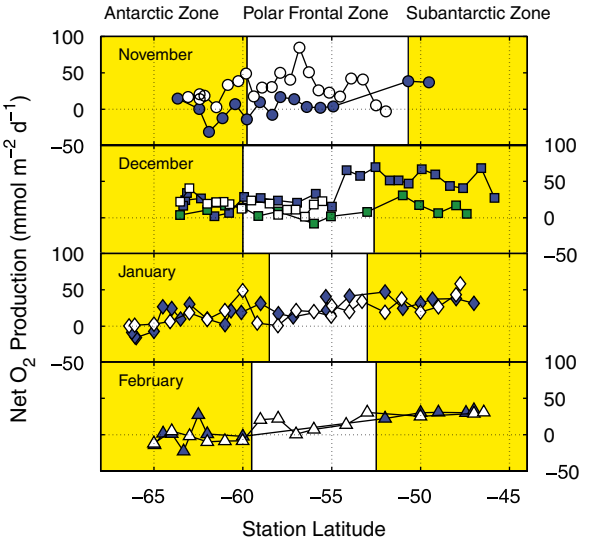

Fig. 10. Seasonal net O_2 production rates south of New Zealand, including mixed layer stations within the Subantarctic Zone, Polar Frontal Zone, and Antarctic Zone. Note the predominance of net autotrophic conditions throughout most of the ACC, the maximum December values within the Subantarctic, and the northward increase in net O_2 production during December through February.

The various production estimates access different scales of time and space, and sometimes include different processes. New production (from $^{15}NO_3^-$ uptake) and POC flux estimates (from ^{234}Th) exclude DOC production, which is included in the other measurements. Net O_2 production (ΔO_2) and new production (^{15}N) are measured using bottle incubation methods and reflect fluxes over 24 h. Our $\Delta(O_2/Ar)$ values integrate over ~1 week, ^{234}Th-POC fluxes average over ~1 month, and seasonal drawdown estimates average over the growing season. Bottle incubations reflect local rates, while estimates based on the drawdown of ^{234}Th and nutrients reflect fluxes over large spatial scales. Calculations of Schlitzer (2002) represent nutrient remineralization rates below the euphotic zone. His fluxes integrate over spatial scales of hundreds of kilometers and timescales of decades. Hence exact agreement is not expected.

In the Subantarctic Zone, Polar Frontal Zone, and Antarctic Zone, NCP rates determined in this study (16–36 mmol m^{-2} d^{-1}, respectively) are within the range of the other estimates. Our results thus reinforce these estimates while providing new information on spatial and temporal variability. In the Antarctic Zone, our estimates are towards the lower end of the range of other independent estimates. This result might reflect a combination of temporal variability and attenuation of biological O_2 saturation by upwelling.

To evaluate possible predictors of net O_2 production, we compared the net O_2 production rates to underway SSTs, satellite-derived [chl-*a*] and PAR from SeaWiFS, monthly climatological mixed layer depths (Levitus and Boyer, 1994), annual surface nutrient concentrations (Conkright et al., 1994), and the Behrenfeld and Falkowski (1997) VGPM. The results are shown in Table 6. All correlations were weak ($r \leqslant 0.63$, $r^2 \leqslant 0.4$), a result that could be due to spatial biases, temporal variability, methodological uncertainties, and the mismatch between instantaneous properties and climatology. However, significant correlation with VGPM ($r = 0.62$) and SST ($r = 0.63$) suggests that it may be possible to estimate net O_2 production using remotely sensed properties. Lowest correlations were observed for net O_2 production with climatological mixed layer depth ($r = 0.18$) and [chl-*a*] ($r = 0.34$). Even though NCP was poorly correlated with [chl-*a*], its correlation with VGPM was as strong as with any other mixed layer property. Correlation coefficients for gross production itself were consistently lower than for NCP. To some extent this reflects greater analytical uncertainty in the $^{17}\Delta$ measurement.

Given these limited mixed layer correlations, what then controls the meridional gradients in net O_2 production? Controlling variables that merit attention are the major nutrient concentrations ($[SiO_2]$, $[NO_3^-]$, and $[PO_4^{3-}]$), temperature, mixed layer depth, proximity to upwelling (in terms of subsurface iron input), and aerosol deposition rate (in terms of iron input by mineral aerosol dissolution). $[SiO_2]$ is undoubtedly a critical influence on new, net, or export production given the importance of diatom and silicoflagellate communities in the Southern Ocean. However, our data, and the model results of Schlitzer (2002), suggest that NCP during most of the growing season is lower south of the Polar Front, where waters are always SiO_2-replete. Rather, NCP is generally highest in the SiO_2-depleted waters of the Subantarctic Zone. During much of the summer, most NCP in the Southern Ocean is occurring in SiO_2-depleted waters.

The other major nutrients ($[NO_3^-]$ and $[PO_4^{3-}]$) are not controlling factors: they vary inversely to the NCP gradient and are always replete in our study region. Upwelling would introduce Fe at the

southern margin of our transects, opposite to where NCP is highest. According to Laws et al. (2000), lower SSTs (among other factors) promote higher NCP rates, but we observe highest values at the warmest temperatures. According to the Levitus and Boyer (1994) climatology, mixed layer depth is not simply related to the NCP gradient, and it too is unlikely to be a major factor leading to higher NCP in the north. However, mixed layer depth is highly variable and its definition is arbitrary. It may be that net production will share variance with instantaneous MLD, or the climatological values defined in another way. MLD thus merits more attention.

One property that could qualitatively account for the net O_2 production gradient is mineral aerosol Fe input. A range of modeling studies integrate the primary factors controlling dust transport and provide strong evidence that aerosol deposition in our study regions is highest at the northern margin (e.g., Ginoux et al., 2001). It remains controversial, however, whether the magnitude of the iron source from aerosol dissolution is adequate to support net O_2 production at the rates we observe. Two recent studies illustrate the range of estimates: Fung et al. (2000) calculate that most NCP in the Subantarctic is fertilized by aerosol iron input, whereas Gregg et al. (2003) calculates that the proximal aerosol source is too small to have a significant impact on dissolved iron concentrations. So the cause of the meridional gradient in net O_2 production remains unresolved.

4.3. Southern ocean net/gross productivity estimates

In Fig. 6 we plot $^{17}\Delta$ (the measure of gross production) versus $\Delta(O_2/Ar)$ (the measure of net production) to document Southern Ocean net/gross variability. The plotted values are aggregated data where values are averaged by transit and zone; error bars represent standard error. Superimposed on these plots are isolines of constant net/gross production. The results were calculated by excluding samples with $\Delta(O_2/Ar) < -0.5\%$, which we believe are influenced by vertical mixing. This cutoff point eliminates most undersaturated samples but allows for analytical uncertainty when $\Delta(O_2/Ar)$ values are close to 0%. As noted above, mixing may attenuate biological O_2 saturation in the Antarctic Zone and artificially lower net production values.

For the majority of the open Southern Ocean, N/G O_2 production ratios vary from 0 to 0.3. No

Table 6
Correlation matrix of mixed layer properties, expressed as r values

	Gross	Net	N/G	VGPM	MLD	$[NO_3]$	$[PO_4]$	$[SiO_4]$	[Chl *a*]	PAR	SST
Gross	1	0.625	−0.266	0.335	0.292	−0.284	−0.388	−0.315	0.100	0.238	0.403
Net	0.625	1	0.495	0.621	0.178	−0.611	−0.554	−0.495	0.335	0.546	0.626
N/G	−0.266	0.495	1	0.343	0.002	−0.293	−0.358	−0.348	0.228	0.326	0.351
VGPM	0.335	0.621	0.343	1	−0.157	−0.492	−0.413	−0.273	0.809	0.527	0.539
MLD	0.292	0.178	0.002	−0.157	1	0.157	−0.017	−0.034	−0.162	−0.160	−0.024
$[NO_3]$	−0.284	−0.611	−0.293	−0.492	0.157	1	0.806	0.686	−0.090	−0.444	−0.907
$[PO_4]$	−0.388	−0.554	−0.358	−0.413	−0.017	0.806	1	0.623	−0.085	−0.374	−0.821
$[SiO_4]$	−0.315	−0.495	−0.348	−0.273	−0.034	0.686	0.623	1	0.067	−0.513	−0.804
[Chl *a*]	0.100	0.335	0.228	0.809	−0.162	−0.090	−0.085	0.067	1	0.153	0.184
PAR	0.238	0.546	0.326	0.527	−0.160	−0.444	−0.374	−0.513	0.153	1	0.467
SST	0.403	0.626	0.351	0.539	−0.024	−0.907	−0.821	−0.804	0.184	0.467	1

All results were averaged by zone for each transit (SAZ, PFZ, and AZ), and the parameters included in the calculation are given below. Gross: gross O_2 production rate from $^{17}\Delta$ observations and gas transfer velocity parameterization (mmol m^{-2} day^{-1}). Net: net O_2 production from $\Delta(O_2/Ar)$ observations and gas transfer velocity parameterization (mmol m^{-2} day^{-1}). N/G: net/gross ratio calculated from $^{17}\Delta$ and $\Delta(O_2/Ar)$ observations and the steady-state model. VGPM: ^{14}C production rate estimated from the Behrenfeld and Falkowski (1997) Vertically Generalized Productivity Model (mmol m^{-2} day^{-1}). MLD: mixed layer depth taken from the monthly climatology of Levitus and Boyer (1994) (m). $[NO_3^-]$: surface nitrate concentrations taken from the annual data set of Conkright et al. (1994) (μmol L^{-1}). $[PO_4]$: surface phosphate concentrations taken from the annual data set of Conkright et al. (1994) (μmol L^{-1}). $[SiO_4]$: surface silicic acid concentrations taken from the annual data set of Conkright et al. (1994) (μmol L^{-1}). [Chl *a*]: monthly mean surface chlorophyll a concentrations taken from SeaWiFS (mg m^{-3}). PAR: monthly mean photosynthetically active radiation taken from SeaWiFS (Einstein m^{-2} day^{-1}). SST: sea surface temperature measured from shipboard underway systems (°C). SeaWiFS data are provided by the Goddard Earth Sciences Data and Information Services Center/Distributed Active Archive Center (Code 902) at the Goddard Space Flight Center, Greenbelt, MD (http://daac.gsfc.nasa.gov).

systematic shift in the N/G ratio is observed between the Subantarctic Zone (mean $N/G = 0.14 \pm 0.01$), Polar Frontal Zone (mean $N/G = 0.16 \pm 0.06$), and Antarctic Zone (mean $N/G = 0.11 \pm 0.08$). Fig. 6 shows that net and gross O_2 production rates covary ($r = 0.63$), and there is no systematic change in N/G from low to high productivity regions. About two-thirds of our aggregated N/G ratios are within the range $0.1 \leqslant N/G \leqslant 0.3$. Analyses of variance (Table 6) reveal that no strong correlation exists between the N/G ratio and other mixed layer parameters that vary across the ACC. For example, $r < 0.36$ for SST, $[NO_3^-]$, $[SiO_4^{2-}]$, and PAR. N/G is most strongly correlated with NCP ($r = 0.5$). Random errors would, of course, introduce some covariance between NCP and the N/G ratio.

The mean N/G values for the three zones are generally representative of austral summer conditions within the open Southern Ocean. As discussed by Hendricks et al. (2004), *f* ratios determined by the relative uptake of new (NO_3^-) versus total ($NO_3^- + NH_3 +$ urea) nitrogen offer a useful comparison to the O_2-based N/G ratios. The ^{15}N incubation method quantifies the rate of new and regenerated production by incubating samples and measuring the incorporation of ^{15}N labeled nitrate, ammonium, and urea into particulate organic nitrogen. For this comparison, we convert the ^{15}N *f* ratio (new/total) to N/G ratios, assuming steady-state conditions (new = NCP), applying the Redfield C:N ratio (6.6), and utilizing the measured relationship between total N assimilation and ^{14}C productivity (mean = 6.4, McCarthy et al., 1996). The ^{15}N *f* ratio thus approximately equals the ratio of net carbon assimilation to ^{14}C productivity. We assume a photosynthetic quotient of 1.4 (net C production = net O_2 production/1.4, Laws, 1991) and a slope for the gross O_2–^{14}C productivity relationship of 2.7 ($m = 2.7$, Marra, 2002). Then the O_2 N/G ratio multiplied by 2.7/1.4 equals the *f* ratio determined by the ^{15}N incubation method. Following the conversion, the *f* ratios as calculated from O_2 N/G production ratios range from 0.27 (Subantarctic Zone) to 0.31 (Polar Frontal Zone).

Comparison of Southern Ocean *f* ratios determined by the ^{15}N and O_2 methods show satisfactory agreement. Sambrotto and Mace (2000) reported *f* ratios from 0.05 to 0.3 along 170°W (excluding the $f = 0.5$ outlier at 57°S). They found no consistent meridional gradient between the Subantarctic and Polar Frontal Zones (see their Fig. 7). They did observe elevated *f* ratios, reaching 0.3, at the December ice edge. Elskens et al. (2002) observed a mean *f* ratio of 0.3 along 142°E, with no significant difference between the Subantarctic and Polar Frontal Zones. Finally, Savoye et al. (2004) reported *f* ratios between 0.33 and 0.69 between 140°E and 145°E, with highest values south of the Polar Frontal Zone. Within the PFZ and SAZ, they observed *f* ratios ranging from 0.33 to 0.56.

Elevated *f* ratios observed by Elskens et al. (2002) and Savoye et al. (2004) within the Antarctic Zone and Marginal Ice Zone agree with the expected predominance of diatom and flagellate communities resulting from stratification. The retreating ice edge may also be an Fe source (Buesseler et al., 2003), resulting in greater assimilation of NO_3^- relative to NH_4^+. Maximum *f* ratios (ca. 0.7) were reported by Savoye et al. (2004) in this region, associated with maximum [chl-*a*] and N-uptake rates. Unfortunately, we cannot determine production rates and *f* ratios in the Marginal Ice Zone because persistent upwelling introduces O_2-undersaturated waters into the mixed layer.

Laws et al. (2000) argued that net/gross production increases with lower temperatures because respiration rates fall faster than photosynthesis rates. Globally there is strong evidence for this temperature dependence. Within the Southern Ocean, however, our data suggest that temperature does not have a dominant influence on net/gross ratios.

5. Conclusions

In this paper, we report a major new data set characterizing rates of net and gross production in the Southern Ocean south of New Zealand, south of Australia, south of Africa, and across the Drake Passage. The approach we used, based on biological O_2 saturation and the triple isotope composition of dissolved O_2, is free of artifacts associated with bottle incubations. Like all ocean biogeochemical rate measurements, it has important limitations. Uncertainties from analytical errors and gas exchange coefficients are large, one must assume constant production in the recent period before sampling, and the possibility of upwelling suggests that our Antarctic Zone NCP data represent minimum estimates.

These limitations notwithstanding, the productivity signal and its variability within the Southern

Ocean are large, and several features persist throughout the austral summer mixed layer:

(1) Gross O_2 production rates inferred from $^{17}\Delta$ measurements show a significant meridional gradient between Australia and Antarctica (higher to the north) and greater variability south of New Zealand. Gross O_2 production rates within the Drake Passage are lower than in the western Pacific sector. The gross O_2 production rates are significantly higher than predicted from the Behrenfeld and Falkowski (1997) VGPM algorithm and the empirical ^{14}C–gross O_2 production relationship measured elsewhere (slope = 2.7). Observed gross and net O_2 production are only weakly correlated with surface [chl-*a*], a principal determinant of modeled primary production rates.
(2) Net O_2 production rates calculated from mixed layer $\Delta(O_2/Ar)$ similarly increase from the south to north; the trend is strongest south of New Zealand and Australia from December to February. South of New Zealand, highest net O_2 production rates were consistently observed within the Subantarctic Zone in December 2002, reaching 86 mmol m^{-2} d^{-1}. There is significant interannual and spatial variability in this region, where our data set is most extensive.
(3) Elevated rates of net O_2 production to the north coincide with lower major nutrient concentrations, warmer SSTs, and increasing distance from the site of upwelling, all factors that would normally be linked with diminished NCP. High rates to the north coincide with an increased aerosol Fe source, but it is not clear if the magnitude of this source can support the net O_2 production rates calculated here.
(4) When our dataset south of New Zealand is averaged, *f* ratios estimated from dual $\Delta(O_2/Ar)$ and $^{17}\Delta$ measurements range from 0.27 in the Subantarctic Zone to 0.31 in the Polar Frontal Zone, within the range of most previous ^{15}N incubation estimates (Elskens et al., 2002; Sambrotto and Mace, 2000). No meridional N/G gradient is observed across the ACC. Our estimate of N/G ratios within the Antarctic Zone can be compromised by both local upwelling or advection of undersaturated waters from the retreating ice margin.

The mixed layer productivity estimates presented here offer new insights regarding the magnitude and variability of Southern Ocean gross and net O_2 production, notably a meridional gradient in gross and net O_2 production and an approximately two-fold difference between measured and remotely sensed (using VGPM) gross O_2 production. These observations are limited by our methodological uncertainties, the variable space and time scales inherent in each method, and the limited existing database. For the $^{17}\Delta$ and $\Delta(O_2/Ar)$ tracers, reduced analytical uncertainty and constrained gas exchange rates will greatly improve the mixed layer flux estimates. For the Behrenfeld and Falkowski (1997) productivity model, new empirical estimates of the chlorophyll-normalized carbon assimilation rate within the Southern Ocean might better constrain primary production rates at low SSTs and replete nutrient availability. Despite these limitations, tracer observations and productivity models clearly show significant natural variability in Southern Ocean productivity throughout the austral summer and its potential response to external forcing.

Acknowledgments

The officers and crew of the Southern Ocean research vessels utilized in this study are gratefully acknowledged, including the RVIB *Nathaniel B. Palmer*, ASRV *Laurence M. Gould*, USCG *Polar Star*, R/V *Melville*, R/V *Revelle*, and R/V *Polarstern*. Many research groups collected underway samples for this project (Table 2). Their efforts made this work possible. Logistical support was provided by the United States Antarctic Program, notably Don Michaelson and Karl Newyear of Raytheon Polar Services Company. Funding was provided by NASA grant NAG5-11301 to M.L.B. and P.G.F. and by the Gary Comer Family Foundation, and postdoctoral support was provided by a Harry Hess Fellowship (M.K.R.).

Appendix A. Supplementary materials

Supplementary data associated with this article can be found in the online version at doi:10.1016/j.dsr.2007.02.007.

References

Angert, A., Rachmilevitch, S., Barkan, E., Luz, B., 2003. Effects of photorespiration, the cytochrome pathway, and the alternative pathway on the triple isotopic composition of atmospheric O_2. Global Biogeochemical Cycles 17 (1) Art. No. 1030.

Barkan, E., Luz, B., 2003. High precision measurements of $^{17}O/^{16}O$ and $^{18}O/^{16}O$ of O_2 and O_2/Ar in air. Rapid Communications in Mass Spectrometry 17, 2809–2814.

Behrenfeld, M.J., Falkowski, P.G., 1997. Photosynthetic rates derived from satellite-based chlorophyll concentration. Limnology and Oceanography 42 (1), 1–20.

Behrenfeld, M.J., Esaias, W.E., Turpie, K.R., 2002. Assessment of primary production at the global scale. In: Williams, P.J.l.B., Thomas, D.N., Reynolds, C.S. (Eds.), Phytoplankton Productivity: Carbon Assimilation in Marine and Freshwater Ecosystems. Blackwell, Malden, MA, p. 386.

Belkin, I.M., Gordon, A.L., 1996. Southern Ocean fronts from the Greenwich meridian to Tasmania. Journal of Geophysical Research—Oceans 101 (C2), 3675–3696.

Benson, B.B., Krause, D., 1984. The concentration and isotopic fractionation of oxygen dissolved in fresh water and seawater in equilibrium with the atmosphere. Limnology and Oceanography 29 (3), 620–632.

Blunier, T., Barnett, B., Bender, M.L., Hendricks, M.B., 2002. Biological oxygen productivity during the last 60,000 years from triple oxygen isotope measurements. Global Biogeochemical Cycles 16 (3) Art. No. 1029.

Bourassa, M.A., Legler, D.M., O'Brien, J.J., Smith, S.R., 2003. SeaWinds validation with research vessels. Journal of Geophysical Research—Oceans 108 (C2) Art. No. 3019.

Boyd, P.W., Watson, A.J., Law, C.S., Abraham, E.R., Trull, T., 2000. A mesoscale phytoplankton bloom in the polar Southern Ocean stimulated by iron fertilization. Nature 407, 695–702.

Buesseler, K.O., Ball, L., Andrews, J., Cochran, J.K., Hirschberg, D.J., Bacon, M.P., Fleer, A., Brzezinski, M., 2001. Upper ocean export of particulate organic carbon and biogenic silica in the Southern Ocean along 170°W. Deep-Sea Research II 48 (19–20), 4275–4297.

Buesseler, K.O., Barber, R.T., Dickson, M.L., Hiscock, M.R., Moore, J.K., Samrotto, R., 2003. The effect of marginal ice-edge dynamics on production and export in the Southern Ocean along 170°W. Deep-Sea Research II 50, 579–603.

Buesseler, K.O., Andrews, J.E., Pike, S.M., Charette, M.A., Goldson, L.E., Brzezinski, M.A., 2005. Particle export during the Southern Ocean iron experiment (SOFeX). Limnology and Oceanography 50, 311–327.

Coale, K.H., Coale, K.H., Johnson, K.S., Chavez, F.P., Buesseler, K.O., Barber, R.T., Brzezinski, M.A., Cochlan, W.P., Millero, F.J., Falkowski, P.G., Bauer, J.E., Wanninkhof, R.H., Kudela, R.M., Altabet, M.A., Hales, B.E., Takahashi, T., Landry, M.R., Bidgare, R.R., Wang, X.J., Chase, Z., Strutton, P.G., Friederich, G.E., Gorbunov, M.Y., Lance, V.P., Hilting, A.K., Hiscock, M.R., Demarest, M., Hiscock, W.T., Sullivan, K.F., Tanner, S.J., Gordon, R.M., Hunter, C.N., Elrod, V.A., Fitzwater, S.E., Jones, J.L., Tozzi, S., Cooper, D., Timothy, D., Brown, S.L., Selph, K.E., Sheridan, C.C., Twining, B.S., Johnson, Z.I., 2004. Southern Ocean iron enrichment experiment: carbon cycling in high- and low-Si waters. Science 304 (5669), 408–414.

COESA, 1976. US Standard Atmosphere, 1976. National Aeronautics and Space Administration, Washington.

Conkright, M., Levitus, S., Boyer, T., 1994. World Ocean Atlas 1994 Volume 1: Nutrients. US Department of Commerce, Washington, DC.

Craig, H., Hayward, T., 1987. Oxygen supersaturation in the ocean—biological versus physical contributions. Science 235 (4785), 199–202.

Dickson, M.L., Orchardo, J., 2001. Oxygen production and respiration in the Antarctic Polar Front region during the austral spring and summer. Deep-Sea Research II 48 (19–20), 4101–4126.

Elskens, M., Baeyens, W., Cattaldo, T., Dehairs, F., Griffiths, B., 2002. N uptake conditions during summer in the Subantarctic and Polar Frontal Zones of the Australian sector of the Southern Ocean. Journal of Geophysical Research—Oceans 107 (C11) Art. No. 3182.

Emerson, S., 1987. Seasonal oxygen cycles and biological new production in surface waters of the Subarctic Pacific Ocean. Journal of Geophysical Research—Oceans 100 (C8), 15873–15887.

Emerson, S., Quay, P., Stump, C., Wilbur, D., Knox, M., 1991. O_2, Ar, N_2, and ^{222}Rn in surface waters of the subarctic Pacific Ocean: net biological O_2 production. Global Biogeochemical Cycles 5, 49–69.

Emerson, S., Quay, P.D., Stump, C., Wilbur, D., Schudlich, R., 1995. Chemical tracers of productivity and respiration in the subtropical Pacific Ocean. Journal of Geophysical Research—Oceans 100 (C8), 15873–15887.

Eppley, R.W., Peterson, B.J., 1979. Particulate organic matter flux and planktonic new production in the deep ocean. Nature 282 (5740), 677–680.

Fung, I.Y., et al., 2000. Iron supply and demand in the upper ocean. Global Biogeochemical Cycles 14 (1), 281–295.

Gao, Y.Q., Marcus, R.A., 2001. Strange and unconventional isotope effects in ozone formation. Science 293 (5528), 259–263.

Gervais, F., Riebesell, U., Gorbunov, M.Y., 2002. Changes in primary productivity and chlorophyll a in response to iron fertilization in the Southern Polar Frontal Zone. Limnology and Oceanography 47 (5), 1324–1335.

Ginoux, P., Chin, M., Tegen, I., Prospero, J.M., Holben, B., Dubovik, O., Lin, S.J., 2001. Sources and distributions of dust aerosols simulated with the GOCART model. Journal of Geophysical Research 106 (D7), 20255–20273.

Gregg, W.W., Ginoux, P., Schopf, P.S., Casey, N.W., 2003. Phytoplankton and iron: validation of a global three-dimensional ocean biogeochemical model. Deep-Sea Research II 50 (22–26), 3143–3169.

Guy, R.D., Fogel, M.L., Berry, J.A., 1993. Photosynthetic fractionation of the stable isotopes of oxygen and carbon. Plant Physiology 101, 37–47.

Hendricks, M.B., Bender, M.L., Barnett, B.A., 2004. Net and gross O_2 production in the Southern Ocean from measurements of biological O_2 supersaturation and its triple isotope composition. Deep Sea Research I 51 (11), 1541–1561.

Hiscock, M.R., Marra, J., Smith, W.O., Goericke, R., Measures, C., Vink, S., Olson, R.J., Sosik, H.M., Barber, R.T., 2003. Primary productivity and its regulation in the Pacific Sector of the Southern Ocean. Deep-Sea Research II 50 (3–4), 533–558.

Kalnay, E., et al., 1996. The NCEP/NCAR 40-year reanalysis project. Bulletin of the American Meteorological Society 77 (3), 437–471.

Kiddon, J., Bender, M.L., Marra, J., 1993. Isotopic fractionation of oxygen by respiring marine organisms. Global Biogeochemical Cycles 7 (3), 679–694.

Kirkwood, D.S., 1992. Stability of solutions of nutrient salts during storage. Marine Chemistry 38, 151–164.

Kroopnick, P.M., Craig, H., 1972. Atmospheric oxygen—isotopic composition and solubility fractionation. Science 175 (4017), 54–55.

Lämmerzahl, P., Röckmann, T., Brenninkmeijer, C.A.M., Krankowsky, D., Mauersberger, K., 2002. Oxygen isotope composition of stratospheric carbon dioxide. Geophysical Research Letters 29 (12).

Laws, E.A., 1991. Photosynthetic quotients, new production, and net community production in the open ocean. Deep-Sea Research 38, 143–167.

Laws, E.A., Falkowski, P.G., Smith, W.O., Ducklow, H., McCarthy, J.J., 2000. Temperature effects on export production in the open ocean. Global Biogeochemical Cycles 14 (4), 1231–1246.

Levitus, S.R., Boyer, T.P., 1994. World Ocean Atlas 1994, Volume 4: Temperature, NOAA Atlas NESDIS 4. US Department of Commerce, Washington.

Lourey, M.J., Trull, T.W., 2002. Seasonal nutrient depletion and carbon export in the Subantarctic and Polar Frontal Zones of the Southern Ocean south of Australia. Journal of Geophysical Research—Oceans 106 (C12), 31463–31487.

Luz, B., Barkan, E., 2005. The isotopic ratios $^{17}O/^{16}O$ and $^{18}O/^{16}O$ in molecular oxygen and their significance in biogeochemistry. Geochimica et Cosmochimica Acta 69 (5), 1099–1110.

Luz, B., Barkan, E., 2000. Assessment of oceanic productivity with the triple-isotope composition of dissolved oxygen. Science 288, 2028–2031.

Ma, C., Shero, E., Verma, N., Gilbert, S.L., Shadman, F., 1995. Permeation of moisture and oxygen through polymeric O-rings. Journal of IES 38 (2), 43–46.

Marra, J., 2002. Approaches to the measurement of plankton production. In: Williams, P.J.l.B., Thomas, D.N., Reynolds, C.S. (Eds.), Phytoplankton Productivity: Carbon Assimilation in Marine and Freshwater Ecosystems. Blackwell, Oxford, p. 386.

Martin, J.H., 1990. Glacial–interglacial CO_2 change: the iron hypothesis. Paleoceanography 5 (1), 1–13.

McCarthy, J.J., Garside, C., Nevins, J.L., Barber, R.T., 1996. New production along 140°W in the equatorial Pacific during and following the 1992 El Niño event. Deep-Sea Research II 43 (4–6), 1065–1093.

Miller, M.F., 2002. Isotopic fractionation and the quantification of ^{17}O anomalies in the oxygen three-isotope system: an appraisal and geochemical significance. Geochimica Cosmochimica Acta 66 (11), 1881–1889.

Millero, F.J., Poisson, A., 1981. International one-atmosphere equation of state of seawater. Deep-Sea Research 28A (6), 625–629.

Morrison, J.M., Gaurin, S., Codispoti, L.A., Takahashi, T., Millero, F.J., Gardner, W.D., Richardson, M.J., 2001. Seasonal evolution of hydrographic properties in the Antarctic Circumpolar Current at 170°W during 1997–1998. Deep-Sea Research II 48 (19–20), 3943–3972.

Nelson, Anderson, R.F., Barber, R.T., Brzezinski, M.A., Buesseler, K.O., Chase, Z., Collier, R.W., Dickson, M.L., Francois, R., Hiscock, M.R., Honjo, S., Marra, J., Martin, W.R., Sambrotto, R.N., Sayles, F.L., Sigmon, D.E., 2002. Vertical budgets for organic carbon and biogenic silica in the Pacific sector of the Southern Ocean, 1996–1998. Deep-Sea Research II 49 (9–10), 1645–1674.

Orsi, A.H., Whitworth, T.W., Nowlin, W.D., 1995. On the meridional extent and fronts of the Antarctic Circumpolar Current. Deep-Sea Research I 42 (5), 641–673.

Quay, P.D., Emerson, S., Wilbur, D., Stump, C., Knox, M., 1993. The $\delta^{18}O$ of dissolved O_2 in the surface waters of the Subarctic Pacific—a tracer of biological productivity. Journal of Geophysical Research—Oceans 98 (C5), 8447–8458.

Sambrotto, R.N., Mace, B.J., 2000. Coupling of biological and physical regimes across the Antarctic Polar Front as reflected by nitrogen production and recycling. Deep-Sea Research II 47 (15–16), 3339–3367.

Sarmiento, J.L., Gruber, N., Brzezinski, M.A., Dunne, J.P., 2004. High-latitude controls of thermocline nutrients and low latitude biological productivity. Nature 427 (6969), 56–60.

Savoye, N., Dehairs, F., Elskens, M., Cardinal, D., Kopczynska, E.E., Trull, T.W., Sright, S., Baeyens, W., Griffiths, F.B., 2004. Regional variation of spring N-uptake and new production in the Southern Ocean. Geophysical Research Letters 31 (3).

Schlitzer, R., 2002. Carbon export fluxes in the Southern Ocean: results from inverse modeling and comparison with satellite-based estimates. Deep-Sea Research II 49 (9–10), 1623–1644.

Sigman, D.M., Boyle, E.A., 2000. Glacial/interglacial variations in atmospheric carbon dioxide. Nature 407, 859–869.

Spitzer, W.S., Jenkins, W.J., 1989. Rates of vertical mixing, gas exchange, and new production—estimates from seasonal gas cycles in the upper ocean near Bermuda. Journal of Marine Research 47 (1), 169–196.

Sturm, P., Leuenberger, M., Sirignano, C., Neubert, R.E.M., Meijer, H.A.J., Langenfleds, R., Brand, W.A., Tohjima, Y., 2004. Permeation of atmospheric gases through polymer O-rings used in flasks for air sampling. Journal of Geophysical Research—Atmosphere 109 (D4) Art. No. D04309.

Thiemens, M.H., Heidenreich, J.E., 1983. The mass-independent fractionation of oxygen: a novel isotope effect and its possible cosmochemical implications. Science 219, 1073–1074.

Thiemens, M.H., Jackson, T.L., Brenninkmeijer, C.A.M., 1995. Carbon dioxide and oxygen-isotope anomalies in the mesosphere and stratosphere. Science 270, 969–972.

Wang, X.J., Matear, R.J., Trull, T.W., 2001. Modeling seasonal phosphate export and resupply in the Subantarctic and Polar Frontal Zones in the Australian sector of the Southern Ocean. Journal of Geophysical Research—Oceans 106 (C12), 31525–31541.

Wanninkhof, R., 1992. Relationship between wind-speed and gas-exchange over the ocean. Journal of Geophysical Research 97 (C5), 7373–7382.

Weiss, R.F., 1970. The solubility of nitrogen, oxygen, and argon in water and seawater. Deep-Sea Research 17, 721–735.

Yung, Y.L., Lee, A.Y.T., Irion, F.W., DeMore, W.B., Wen, J., 1997. Carbon dioxide in the atmosphere: isotopic exchange with ozone and its use as a tracer in the middle atmosphere. Journal of Geophysical Research—Atmosphere 102 (D9), 10857–10866.